Workshop on
Fundamental Aspects of Geophysical Turbulence II
at NCAR 5-7 August 2015, Boulder, CO, U.S.A

Damon Room, NCAR Mesa Laboratory
Meeting Agenda

Wednesday August 5

8:45-9:00 Opening remarks

9:00-9:55 James Riley
On the dynamics of turbulent/non-turbulence interfaces in stably-stratified fluids

10:00-10:55 Joseph Werne
Parameter-dependent morphology in Kelvin-Helmholtz layers and their implications for modeling stratified turbulence

Coffee Break

11:20-12:05 Yukio Kaneda
Length scales in turbulent flows

Outdoor observations (a working lunch)

13:30-14:25 James McWilliams
Oceanic submesoscale dynamics: Dense filament frontogenesis & arrest by boundary layer turbulence

14:30-15:25 Subhas Karan Venayagamoorthy
A framework for the prediction of turbulent diapycnal mixing in stably stratified geophysical flows

Coffee Break

15:55-16:50 David Richter
How far upscale does a dispersed phase influence turbulence?

Reception Mesa Lab Cafeteria

19:00 **Bus departs for hotel**

Thursday August 6

9:00-9:55 Peter Davidson
Planetary dynamos driven by helical waves

10:00-10:55 Boris Galperin
Turbulence and waves on a westward jet - an experimental study

Coffee Break

11:20-12:15 Stephen Belcher
The diurnal cycle of the ocean surface boundary layer

Outdoor observations (a working lunch)

13:30-14:25 Charles Meneveau
Synchronization of chaos in fully developed turbulence

14:30-15:25 Harm Jonker
The prediction horizon of convective boundary layers

Coffee Break

15:55-16:50 Gabriel Katul
Co-spectral budgets link energy distributions in eddies to bulk flow properties

17:30 **Bus departs Mesa Lab**
18:00 **Bus departs hotel**
18:30 **Dinner The Med**
21:00 **Bus departs for hotel**

Friday August 7

8:45-9:40 John Finnigan
Canopy-boundary layer coupling in convectively unstable flows:
A tale of interacting instabilities

9:45-10:40 Andreas Muschinski
Optical turbulence: from first principles to working models

Coffee Break

11:00-11:55 Yoshiyui Tsuji
Large and small scale interaction of pressure in turbulent boundary layers

Outdoor observations (a working lunch)

13:10-14:05 Stephen de Bruyn Kops
Classical scaling and intermittency in strongly stratified Boussinesq turbulence

14:10-15:05 Michael Waite
Physical- and eddy-viscosity effects in simulations of stratified turbulence

15:10-15:30 Esa-Matti Tastula
Insights into the performance of the QNSE-EDMF scheme in stable and unstable conditions

End-of-Meeting

Up-the-hill Refreshments Mesa Lab Tree Plaza

17:00 **Bus departs for hotel**

Workshop on
Fundamental Aspects of Geophysical Turbulence II
at NCAR, 5-7 August 2015, Boulder, CO, USA

On the dynamics of turbulent/non-turbulence interfaces in stably-stratified fluids

James J. Riley[1], Tomoaki Watanabe[1], Stephen M. de Bruyn Kops[2] and Peter J. Diamessis[3]
[1] *University of Washington, Seattle, WA 98195, U.S.A*
[2] *University of Massachusetts, Amherst, MA 01003, USA*
[3] *Cornell University, Ithaca, NY 14853, U.S.A.*

Turbulence in stably-stratified fluids is usually localized, such as when an internal wave breaks down into turbulence, the mixing layer of the ocean, a stable atmospheric boundary layer, and many other circumstances. Of considerable interest is the behavior of the turbulence near the interface between the turbulent and non-turbulent regions. This interface is where, for example, the turbulent region can grow into the non-turbulent region by entrainment, and where internal waves are generated and then propagate away from the turbulent region.

The behavior of the turbulent/non-turbulent interface for non-stratified fluids is becoming well-understood, starting with the seminal work of Corrsin and Kistler [1], who, working in wind tunnels, explored turbulent/non-turbulent interfaces in the cases of turbulent boundary layers, turbulent wakes, and turbulent jets. A principal contribution was conceptual; they concluded that the defining characteristic of a turbulent region is its high vorticity, and applied the term 'turbulent' to stochastic rotational fields, as opposed to the irrotational flow outside of the turbulent region. This allowed them to use hot-wired measurements to distinguish the turbulent and non-turbulent regions. Their work has been extended in many ways and to other flows, most recently using direct numerical simulations (see, for example, da Silva et al.[2] for a review of this topic).

It is clear that this definition of turbulence must be extended for turbulence in stably-stratified fluids. First, a field of linear or weakly nonlinear internal waves can be both stochastic and possess vorticity. It is not desirable, however, to define this field as turbulent, since is does not possess other properties usually associated with turbulence, such as intense mixing, high rates of mass transfer, and elevated dissipation rates. We find here that it is useful to extend Corrsin and Kistler's definition of turbulence to apply to stochastic fields with high potential vorticity. Such a field has all the properties which are normally associated with turbulence.

In this study we report on the study of turbulent patches of turbulence in stably-stratified fluids using very high resolution numerical simulations. In particular here we focus on the turbulent/non-turbulent interface of these flows. The simulations are first performed as modeling of the wake of a sphere in a stratified fluid (Abdilghanie and Diamessis[3]). Spectral element methods are used to solve the Navier-Stokes equations, subject to the Boussinesq approximation, on fairly high resolution grids; the simulations are nearly direct numerical simulations, although a weak amount of subgrid-scale modeling is used to maintain numerical stability and accuracy. The flows are initialized to represent as closely as possible to the wakes of a sphere studied by Spedding[4]. The results from these simulations are then interpolated onto an even higher resolution grid and, using Fourier-Spectral methods, the simulations are further run out in time at even higher Reynolds numbers; these simulations, being very well-resolved, are direct numerical simulations.

Figure 1 is a typical plot of the enstrophy field in a vertical cross-section of a wake. In simulations of non-stratified flows (da Silva et al.[2]), following Corrsin and Kistler, the enstrophy is found to be a good marker of the turbulent region. In the present case, however, it is clear that enstrophy is not a good marker for the turbulent region, as it also includes the propagating internal wave field evident in the outer regions of the flow field. In Figure 2 is plotted the potential enstrophy field for the same vertical cross-section at the same time. It is clear that the potential enstrophy field, as expected, has eliminated the internal wave field. We find that it is a good marker for the flow which possesses all the properties of turbulence.

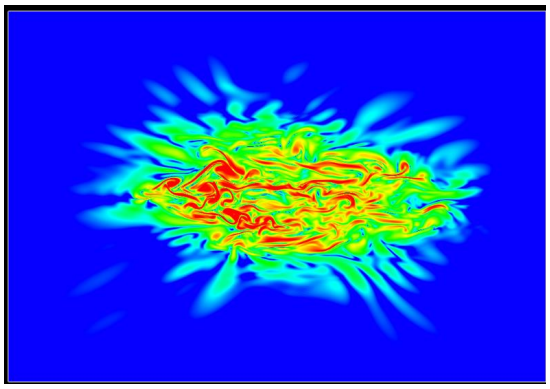

Figure 1: *Typical plot of a vertical cross-section of the enstrophy field.*

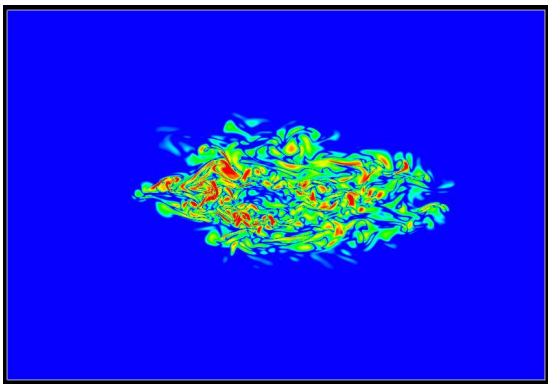

Figure 2: *Vertical cross-section of the potential enstrophy field.*

The results presented will focus on several different times in the decay of the wakes, and at two different Reynolds numbers. Defining the turbulence in the wake in terms of its potential vorticity, along with its dissipation rate, the turbulent/non-turbulent interface is determined, and various quantities are examined in the wake interior, in the interfacial region, and outside the wake. These include the statistical properties of the location of the interfacial region, the properties of the internal waves near the interface and outside the wake region, the local Kolmogorov and Ozmidov scales as well as the Buoyancy Reynolds number, the enstrophy and potential enstrophy budgets, and other quantities of interest.

References

[1] S. Corrsin and A.L. Kistler 1955 *Free-stream boundaries of turbulent flows*, NACA Report **1244**.

[2] C.B. da Silva, J.C.R. Hunt, I. Eames, and J. Westerweel 2014 *Interfacial layers between regions of different turbulence intensity*, Annu. Rev. Fluid Mech. **46**, 567-590.

[3] A.M. Abdilghanie and P.J. Diamessis 2013 *The internal gravity wave field emitted by a stably stratified turbulent wake* J. Fluid Mech. **720**, 104-139.

[4] G.R. Spedding 1997 *The evolution of initially turbulent bluff-body wakes at high internal Froude number*, J. Fluid Mech. **337**, 283-301.

Workshop on
Fundamental Aspects of Geophysical Turbulence II
at NCAR, 5-7 August 2015, Boulder, CO, USA

Parameter-dependent morphology in Kelvin-Helmholtz layers and their implications for modeling stratified turbulence

Joseph Werne[1]
[1] *NorthWest Research Associates, Boulder, Colorado 80301, U.S.A.*

Attempting to parameterize the dynamics and transport properties of stably stratified turbulence is inherently challenging, owing to its spatial intermittency (i.e., organization into layers) and its temporally sporadic nature. Modeling efforts must account for both the differing dynamics of individual layers and the collective effects of their mutual interaction, which is currently not well understood, though progress is being made. To fully attack the problem, three areas of focus must be addressed: 1) We must assess the appropriate parameter ranges of individual layer dynamics that arise naturally (e.g., as a function of altitude, latitude, and season); 2) We must quantify the different statistics and transport characteristics of the parameter ranges observed; and 3) We must decipher their mutual interaction and how that affects their collective behavior.

In this talk I will describe progress along this path by focusing first on recent simulations of the turbulent evolution of isolated shear layers initiated by the Kelvin-Helmholtz instability. These simulations demonstrate that the dynamics, morphology, and turbulent statistics of an isolated shear layer all depend sensitively on the initial Richardson number Ri and Reynolds number Re used. This opens the door to the identification of individual layer characteristics for in-situ and remotely observed layers, even when the observations occur well into the evolving dynamics and not at the initial stage when evaluation of the layer's initial characteristics would be more straightforward. I will give examples of how this is already being done using aircraft, balloon-borne rawindsone, cloud, and airglow data. Suh an ability holds promise for more complete characterization of atmospheric and oceanic turbulence by quantifying the likelihood of observed turbulent-layer properties with altitude, latitude, and season.

Complications arising for interacting layers and coupling to an underlying gravity-wave field will also be discussed.

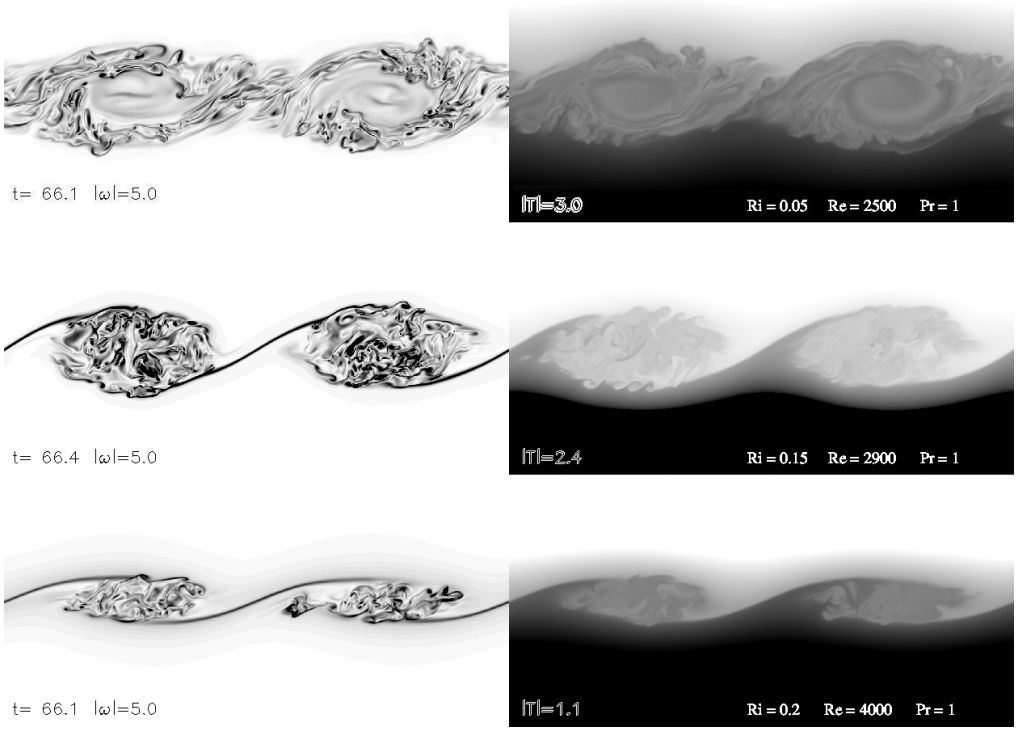

Figure 1: *Snapshop of vorticity (left) and temperature (right) for the Kelvin-Helmholtz (KH) instability for three different Richardson numbers Ri. For weak stratification (Ri=0.05), KH billows are deep, with cores that are stabilized by solid-body rotation, delaying the onset of turbulence in the billow cores. For stronger stratification (Ri=0.20), KH billows are shallow, with cores that immediately succumb to turbulent motion. The differing morphologies and evolutions that result can be used to identify shear-layer parameters.*

References

[1] D. Fritts, G. Baumgarten, K. Wan, J. Werne and T. Lund 2014 *Quantifying Kelvin-Helmholtz instability dynamics observed in noctilucent clouds: 2. Modeling and interpretation of observations*, J. Geophys. Res., Vol 119, pp 9359-9375, doi:10.10 02/2014JD 021833

[2] D. Fritts, K. Wan, J. Werne, T. Lund and J. Hecht 2014 *Modeling the Implications of Kelvin-Helmholtz Instability Dynamics for Airglow Observations*, J. Geophys. Res., Vol 119, doi:10.1002/2014JD021737

[3] D. Wroblewski, J. Werne, O. Cote, O. Hacker and R. Dobosy 2010 *Temperature and velocity structure functions in the upper troposhere and lower stratosphere from aircraft measurements (invited)*, J. Geophys. Res., DOI:10.1029/2010JD014618

[4] J. Werne, D. Fritts, L. Wang, T. Lund and K. Wan 2010 *Atmospheric Turbulence Forecasts for Air Force and Missile Defense Applications (invited)*, *20th DoD HPC User Group Conference* 14-17 June, Schaumburg, IL, DOI:10.1109/HPCMP-UGC.2010.75

[5] F. Ruggiero, A. Mahalov, B. Nichols, J. Werne and D. Wroblewski 2007 *Characterization of High Altitude Turbulence for Air Force Platforms*, *17th DoD HPC User Group Conference* June, Pittsburgh, PA., DOI:10.1109/HPCMP-UGC.2007.15

Workshop on
Fundamental Aspects of Geophysical Turbulence II
at NCAR, 5-7 August 2015, Boulder, CO, USA

Length Scales in Turbulent Flows

Yukio Kaneda[1], Koji Morishita[2], Takashi Ishihara[3] Mitsuo Yokokawa[2], and Atsuya Uno[4]
[1] *Department of Natural Science, Aichi Institute of Technology, Yachikusa 1247, Toyota, 470-0392*
[2] *Department of Computational Science, Kobe University, Rokkodai-cho 1-1, Nada-ku, Kobe, 657-8501*
[3] *Center for Computational Science, Nagoya University, Furo-cho, Chikusa-ku, Nagoya, 464-8603*
[4] *RIKEN Advanced Institute for Computational Science, Kanazawa-ku, Chuo-ku, Kobe, 650-0047*

[Preliminary]
Turbulence is a multi-scale phenomenon involving eddies of a wide range of scales. One of the most characteristic features of high Reynolds number turbulence is the wide separation between the scales, say $\approx L$, where the most energy is and the small scale, say $\approx \ell_d$, where the most energy dissipates. In isotropic incompressible turbulence, the scale ℓ_d is well approximated by the Kolmogorov micro-scale defined as $\eta \equiv (\nu^4/\epsilon)^{1/4}$, in which ϵ and ν are the mean energy dissipation rate per unit mass and the kinematic viscosity, respectively.

There is another length scale called Taylor micro-scale λ. In literature, it is often defined as the length-scale associated with the second order derivative of the longitudinal velocity correlation. In isotropic turbulence, it is given by $\lambda = (15\nu u'^2/\epsilon)^{1/2}$. It has also the following meanings.
(a) mean radius of curvature of the stream lines in isotropic turbulence [1],
(b) thickness of strong thin shear layer in isotropic turbulence [2],
(c) the scale of the so-called detached Q^-events in the log law region of turbulent channel flow [3], and
(d) recent high resolution DNSs up to $R_\lambda \approx 2100$ suggest that it may have another meaning (see below).

[Turbulent Shear Flows – Log Law region]
Consider a turbulent shear flow, and let S_{ij} be the local rate of the strain of the mean flow. Then, a simple dimensional consideration based on the idea of K41 suggests that there is a length scale L_S at which the magnitude of the influence of the mean flow on the distortion of the eddies of size $\approx L_S$ is similar to that due to the non-linear interactions with eddies of similar size, and $L_S = \epsilon^{1/2}/S^{3/2}$ where S is an appropriate norm of S_{ij}. This length scale agrees with that introduced by Corrsin [5], who assumed that the turbulence is isotropic at scales smaller than the scale. There is another length scales, say L_{TL}, defined as $L_{TL} = S/u'$. [4]

It is known that in wall bounded turbulence there is a region in which the mean streamwise velocity U fits well to a simple law (log law), in a certain range depending on Re_τ. According to the DNS data of turbulent channel flow up to $Re_\tau = 5120$[6], ϵ fits well to $\epsilon^+ = 1/(\kappa y^+)$, so that $\eta^+ = (\kappa y^+)^{1/4}$ in the region, where $\kappa \approx 0.4$, the symbol $^+$ denotes the wall unit, and y is the distance from the wall.

In the wavenumber range $1/L_s, 1/L_{TL} \ll k \ll 1/\eta$, one may apply the idea of linear response theory to the second order velocity correlation. It has been shown to be consistent with DNS and experiments.[1,7,8]

[Kolmogorov and Karman Constants]
Karman constant is one of most well-known constants in the theory of turbulence. One may ask, "Can it be estimated theoretically from the first principle, i.e., the Navier-Stokes equation?", or "How can we relate it to the principle?" In this respect, it is to be recalled that Lagrangian spectral closures give a reasonable theoretical estimates for another well-known constant Kolmogorov constant for the K41 spectrum. One may be then tempted to apply such a theory to the log-law region, as in Leslie [9]. In the theory, the two-point velocity correlations $Q_{ij}(x - x', y, y', z - z') =< u_i(x, y, z)u_j(x', y', z') >$ plays a key role, and he assumed a kind of self-similarity form of Q_{ij}. The theory suggests the importance of the $y-$ dependence of characteristic length scale of Q_{ij}.

A recent DNS data analysis suggests that although the assumption of the self-similarity form agrees with the DNS data to a certain degree, the agreement is not very good. The length scales λ_{ii}^m (no summation over i) of Q_{ij} defined similarly to λ in terms of Q_{ij} scales well with $y^{1/2}$, where m denotes the direction x, y or z of the separation vector $\mathbf{x} - \mathbf{x}'$.

The analysis of the closure equation suggests that Karman constant may depend on the geometry of the wall, (channel, single wall, pipe), via the influence of the pressure.

[Isotropic Turbulence]
DNS of almost isotropic turbulence at high R_λ showed a range in which the spectrum $E(k)$ fits well to the -5/3 law, but the slope is a little steeper than -5/3.[10] Such a slope has been also confirmed by recent DNSs of of forced incompressible turbulence in a periodic box with the number of grid points up to 12288^3 performed on the K-computer system.[11] The data suggest that the tilted range is at $k\lambda \sim 1$ and the range is not free from the viscosity. At the run with $R_\lambda \approx 2300$, the wavenumber range $k\lambda \approx 1$ corresponds approximately to the range $k\eta \approx 10^{-2}$. This implies that the wavenumber range with $k\eta \leq 10^{-2}$ or so is not the genuine inertial range, and one need be careful to deduce from the data in such a range the so-called anomalous scaling exponents which are supposed to be viscosity-independent.

This work has been supported partly by JSPS KAKENHI Grant Number (S)24224003 and (C)26400410.

References

[1] Y. Kaneda and K. Morishita 2012 *Small-scale statistics and structure of turbulence – in the light of high resolution direct numerical simulation.* In *Ten Chapters in Turbulence*, edited by P.A. Davidson, Y.Kaneda and K.R.Sreenivasan, pp. 1-42. Cambridge University Press.

[2] T. Ishihara, Y. Kaneda, and J.C.R. Hunt 2013 *Thin shear layers in high Reynolds number turbulence-DNS results.* Flow, Turbulence and Combustion, **91**, 895-929.

[3] A. Lozano-Duran and J. Jimenez 2014 *Time-resolved evolution of coherent structures in turbulent channels: characterization of eddies and cascades* J. Fluid Mech. **759**, 432-471.

[4] J. L. Lumley 1967. *Similarity and the turbulent energy spectrum.* Phys. Fluids, **10**, 855-858.

[5] S. Corrsin 1958 *Local isotropy in turbulent shear flow* Research Memo , 5bb11 (NACA, 1958)

[6] K. Morishita, T. Ishihara and Y. Kaneda 2011 *Small-scale statistics in direct numerical simulation of turbulent channel flow at high-Reynolds number.* J. Phys.: Conference Series, **318**, 022016-1–6.

[7] T. Ishihara, K. Yoshida and Y. Kaneda 2002 *Anisotropic velocity correlation spectrum at small scales in a homogeneous turbulent shear flow.* Phys. Rev. Lett., **88**, Art. No. 154501-1–4.

[8] Y. Tsuji and Y. Kaneda 2012 *Anisotropic pressure correlation spectra in turbulent shear flow.* J. Fluid Mech., **694**, 50-77.

[9] D. C. Leslie 1973 *Developments in the theory of turbulence.* Clarendon Press.

[10] Y. Kaneda, T. Ishihara, M. Yokokawa, K. Itakura and A. Uno 2003 *Energy dissipation rate and energy spectrum in high resolution direct numerical simulations of turbulence in a periodic box.* Phys. Fluids **15**, L21-L24.

[11] T. Ishihara, K. Morishita, M. Yokokawa, A. Uno and Y. Kaneda 2015 *Energy spectra of high Reynolds number turbulence by DNS with up to 12288^3 grid points.* http://meetings.aps.org/Meeting/DFD14/Session/H27.2.

Workshop on
Fundamental Aspects of Geophysical Turbulence II
at NCAR, 5-7 August 2015, Boulder, CO, USA

Oceanic Submesoscale Dynamics: Dense Filament Frontogenesis & Arrest by Boundary Layer Turbulence

James McWilliams[1] and Peter P. Sullivan[2]
[1] *Dept. of Atmospheric and Oceanic Sciences, UCLA, Los Angeles, CA 90095-1565, U.S.A.*
[2] *National Center for Atmospheric Research, Boulder, Colorado 80307-3000, U.S.A.*

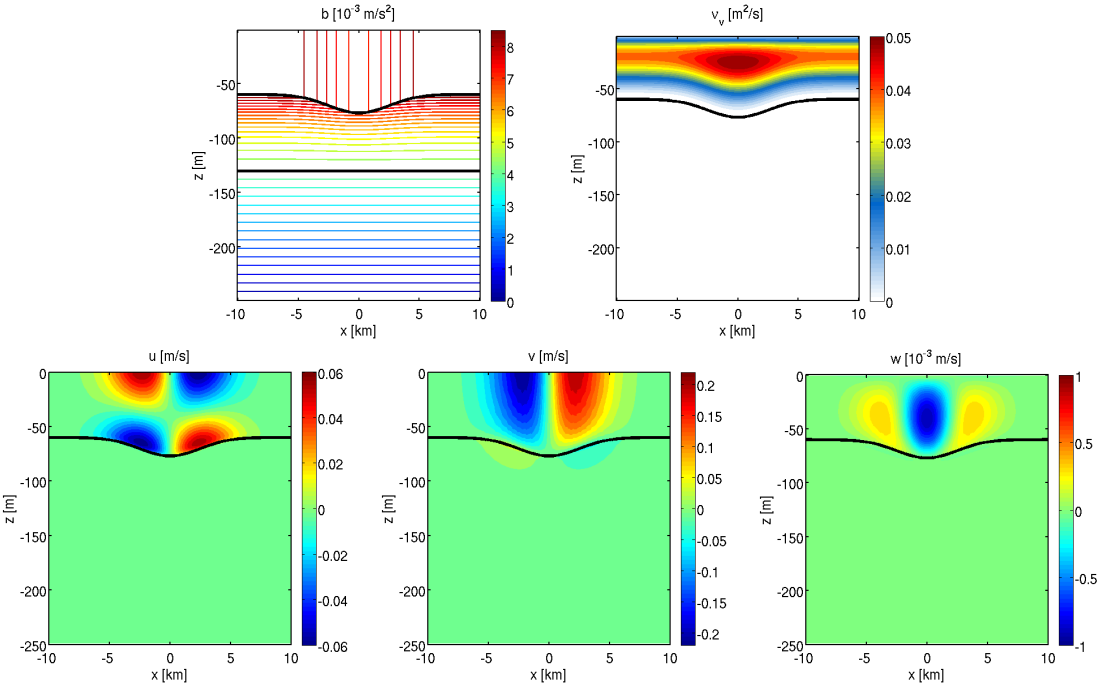

Figure 1: *An idealized submesoscale dense surface filament: (top) buoyancy field and vertical eddy viscosity as prescribed by the K-Profile Parameterization; (bottom) the associated cross-filament, along-filament, and vertical velocities as prescribed in a Turbulent Thermal Wind balance. The black line is the diagnosed boundary layer depth at* $z = -h(x)$. *This secondary circulation is convergent at the surface, hence frontogenetic. The fields are uniform in the perpendicular y-direction.*

A brief overview will be given for submesoscale turbulence in the oceanic surface layer. It is comprised primarily of fronts, dense filaments [1], and coherent vortices created by a forward available energy cascade from oceanic mesoscale eddies (and partly, but not wholly, returned to larger scales by an inverse kinetic energy cascade), with associated strong lateral and diapycnal material mixing.

The primary focus will be on the particular phenomenon of how a dense filament, once formed primarily by classical (mesoscale) strain-induced frontogenesis [2], in the presence of boundary layer turbulence, has an associated secondary circulation (Fig. 1) that satisfies an approximate, quasi-static, incompressible mass and momentum balance that combines buoyancy, pressure-gradient, Coriolis, and vertical momentum mixing forces, called Turbulent Thermal Wind:

$$\begin{aligned} f\hat{\mathbf{z}} \times \mathbf{u}_h &= -\nabla_h \phi + \partial_z \left[\nu_v \partial_z \mathbf{u}_h \right] , \\ \partial_z \phi &= b , \qquad \nabla_h \cdot \mathbf{u}_h + \partial_z w = 0 , \end{aligned}$$

where subscripts h and v denote horizontal and vertical directions, respectively, and $\mathbf{u}_h = (u, v)$.

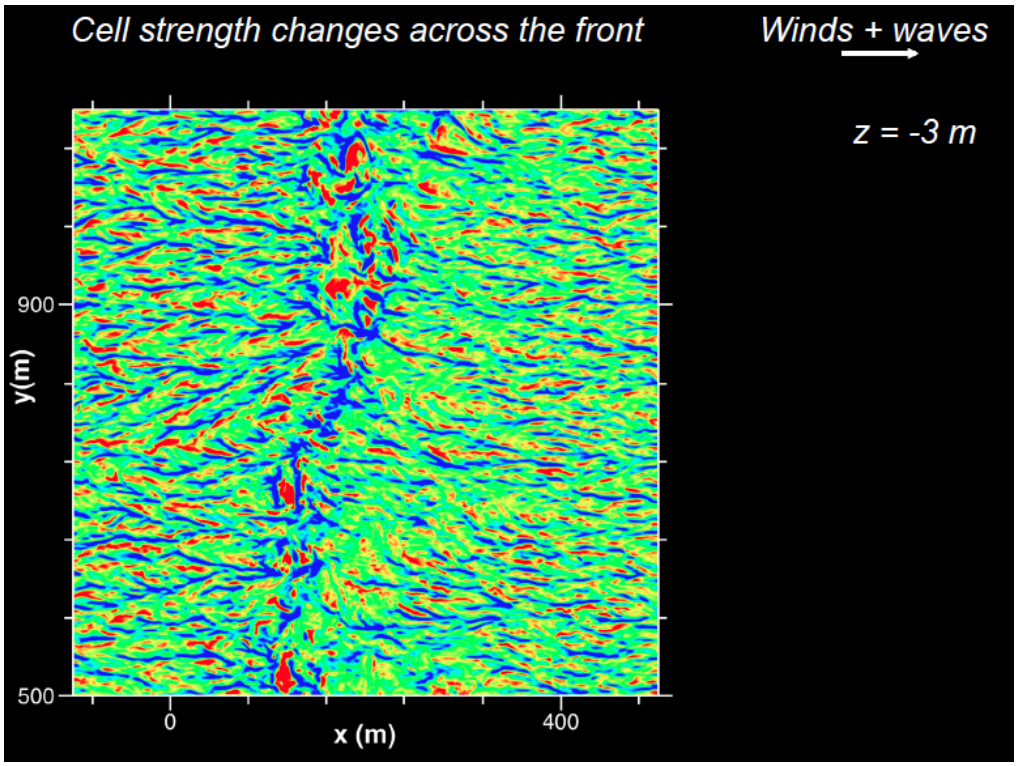

Figure 2: *A spatial zoom of the vertical velocity $w(x, y)$ at $z = -3m$ in a Large-Eddy Simulation of a cold surface filament with surface wind stress and equilibrium wind waves directed to the east. By this time the frontogenesis has created a very narrow filament core that has been arrested primarily by boundary layer turbulent lateral buoyancy and momentum fluxes and has initiated a submesoscale lateral shear instability evident as an along-filament meander. The peak value of the y-averaged vertical vorticity is in excess of $50f$. Notice the strong horizontal inhomogeneity of the small scale turbulent patterns.*

This submesoscale secondary circulation in the cross-filament plane is frontogenetic, and this leads to a super-exponential rate of sharpening of the cross-filament buoyancy and horizontal velocity gradients. Within less than a day, the frontogenesis is arrested at a very small width, $<$ 100 m, primarily by boundary layer turbulence (Fig. 2), with a subsequent slow decay by further turbulent mixing. This phenomenon is examined both in a hydrostatic circulation simulation with parameterized turbulence [3] and in a Large-Eddy Simulation (LES) with resolved turbulent motions. In the LES, for some wind and wave directions, the sharp filament exhibits a submesoscale lateral shear instability, and the boundary layer turbulence is strikingly inhomogeneous in relation to the submesoscale filamentary currents and density stratification.

References

[1] Gula, J., M.J. Molemaker, and J.C. McWilliams, 2014: Submesoscale cold filaments in the Gulf Stream. *J. Phys. Ocean.* **44**, 2617 – 2643.

[2] McWilliams, J.C., F. Colas, & M.J. Molemaker, 2009: Cold filamentary intensification and oceanic surface convergence lines. *Geophys. Res. Lett.* **36**, L18602.

[3] McWilliams, J.C., J. Gula, M.J. Molemaker, L. Renault, & A.F. Shchepetkin, 2015: Filament frontogenesis by boundary layer turbulence. *J. Phys. Ocean.*, in press.

Workshop on
Fundamental Aspects of Geophysical Turbulence II
at NCAR, 5-7 August 2015, Boulder, CO, USA

A framework for the prediction of turbulent diapycnal mixing in stably stratified geophysical flows

Subhas Karan Venayagamoorthy
Department of Civil and Environmental Engineering, Colorado State University, Fort Collins, Colorado 80525-1372, U.S.A.

The prediction of diapycnal (irreversible) mixing in stably stratified geophysical flows such as in the ocean or atmospheric boundary layer, has been the subject of numerous studies over the last few decades. From a practical standpoint, the two key quantities that are essential for estimating turbulent diapycnal mixing in stably stratified flows are: the dissipation rate of the turbulent kinetic energy ϵ and the diapycnal mixing efficiency R_f^*, which is a measure of the amount of turbulent kinetic energy that is irreversibly converted into background potential energy.

A linear relationship between the Thorpe (vertical overturn) length scale L_T and the Ozmidov scale L_O is widely assumed in physical oceanography in order to infer the dissipation rate of turbulent kinetic energy. This approach is particularly attractive since the vertical scales of overturns are easily calculable using a sorting algorithm from inversions in standard density profiles obtained from Conductivity-Temperature-Depth (CTD) measurements in the ocean. Hence L_T is essentially a kinematic scale that provides a description of the turbulence at a given sampling location. On the other hand, L_O is obtained from dimensional reasoning based on the assumption that there is a balance between inertial and buoyancy forces. In other words, the Ozmidov scale is a representative dynamic length scale of the largest eddy that is unaffected by buoyancy. A review of a number of recent studies (in particular [1],[2] & [3]) will be presented in this talk to highlight the lack of a linear relationship between the Thorpe length scale and the Ozmidov scale. These studies indicate that inferred estimates of the dissipation rate of turbulent kinetic energy may be biased high by up to an order of magnitude or more especially for large overturns in the ocean. An alternative framework using a two-dimensional parameter space based on a buoyancy strength parameter NT_L, where N is the buoyancy frequency and $T_L = k/\epsilon$ with k as the turbulent kinetic energy, and a shear strength parameter ST_L, where S is the mean shear rate, will be used to characterize the scaling correspondence of the overturning scale with pertinent turbulent length scales (see Figure 1).

Estimates of turbulent mixing in geophysical settings typically depend on the efficiency at which shear-driven turbulence mixes density across isopycnals. To date, however, no unifying parameterization of diapycnal mixing efficiency (R_f^*) exists due to the variability of natural flows and also due to certain ambiguities that arise from descriptions based on a single parameter. Important ambiguities of some common single-parameter schemes in the context of the multi-parameter framework (as shown in Figure 1) that considers the independent effects of shear, buoyancy, and viscosity will be highlighted. Parameterizations based on the gradient Richardson number (Ri), the turbulent Froude number (Fr_T), and the buoyancy Reynolds number (Re_b) are considered. The diagnostic ability of these parameters is examined using published data from both direct numerical simulations and field observations. In particular, there is an ongoing debate in the oceanographic mixing community regarding the utility of the buoyancy Reynolds number Re_b, particularly with regard to how mixing efficiency and diapycnal diffusivity vary with this parameter. Specifically, is there a universal relationship between the intensity of turbulence (which is given by the turbulent Reynolds number Re_L) and the strength of the stratification (Ri or NT_L) that supports an unambiguous description of mixing efficiency based on Re_b? This is a particularly important question to consider when employing DNS-based parameterizations to describe geophysical turbulence. In the former, high Re_b is most easily achieved with weak stratification due to computational limitations on the turbulent Reynolds number Re_L. In the

latter, however, turbulence can be sustained in the presence of strong stratification due to high Reynolds numbers. For example, consider the geophysical data of Lozovatsky and Fernando [4] plotted in Figure 2 (see [5] for a detailed discussion). In contrast to the predictions in [6] and [7], the field data suggest that the trend of decreasing mixing efficiency may shift toward higher Re_b (into the energetic regime) by at least three orders of magnitude. High mixing efficiency despite high Re_b implies that geophysical flows occupy a high Re_L, high NT_L regime not achieved in the DNS simulations. These findings clearly show that Re_b based parameterizations that are developed for low-Reynolds number experimental flows are not universal or appropriate for geophysical flows.

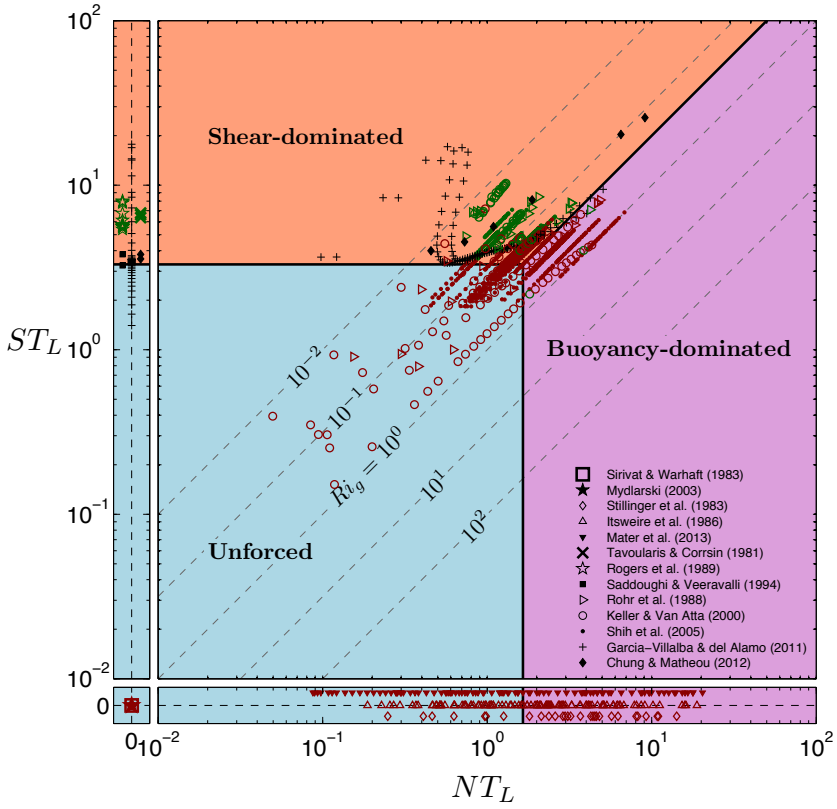

Figure 1: *Parameter space for interpretation of high-Reynolds number turbulence. Growing turbulence ($Dk/Dt > 0$) showed in green, stationary turbulence ($Dk/Dt = 0$) shown in black, and decaying turbulence ($Dk/Dt < 0$) shown in red. Select data points have been offset from $NT_L = 0$ or $ST_L = 0$ for clarity. Lines delineating regimes are first order approximations.*

References

[1] B. D. Mater, S. M. Schaad and S. K. Venayagamoorthy 2013 *Relevance of the Thorpe scale in stably stratified turbulence*, Physics of Fluids **25**, 076604 (2013); doi: 10.1063/1.4813809.

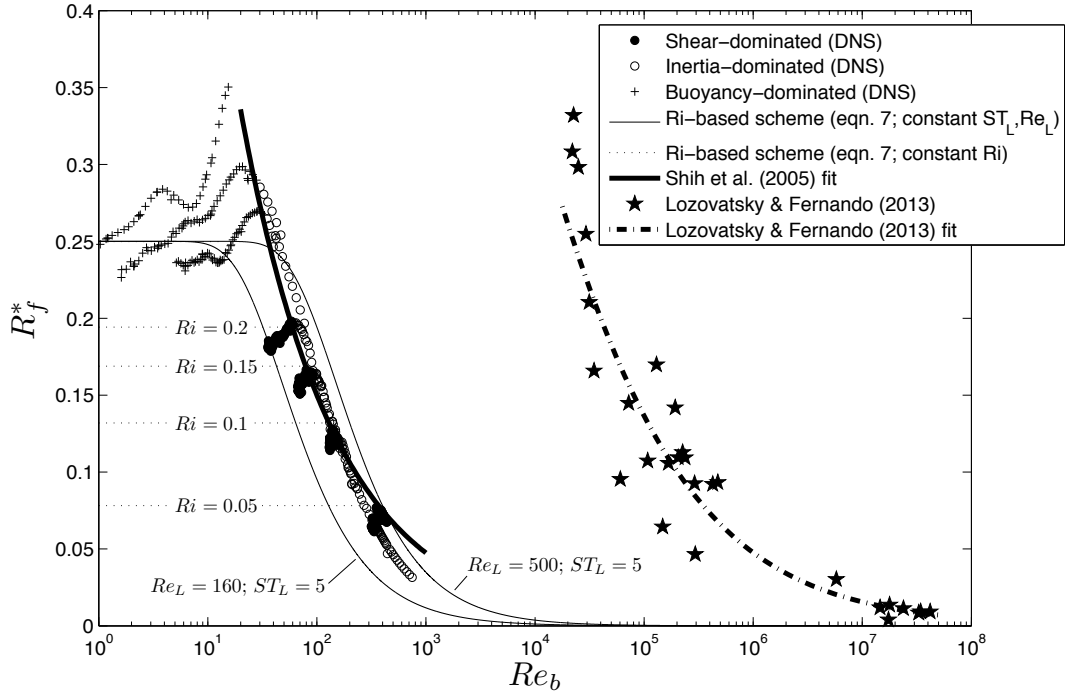

Figure 2: *Diapycnal mixing efficiency, R_f^*, versus the buoyancy Reynolds number, Re_b, for the DNS data of [6]) and the geophysical data of [4]. The Ri-based scheme has been plotted assuming different values of ST_L and Re_L (solid lines) or Ri (dotted lines).*

[2] B. D. Mater and S. K. Venayagamoorthy 2014 *A unifying framework for parameterizing stably stratified shear-flow turbulence*, Physics of Fluids **26**, 036601 (2014) doi: 10.1063/1.4868142.

[3] B. D. Mater, S. K. Venayagamoorthy, L. St. Laurent and J. N. Moum 2015 *Biases in Thorpe scale estimates of turbulence dissipation Part I: Assessments from large-scale overturns in oceanographic data*, Journal of Physical Oceanography **in press**, doi: 10.1175/JPO-D-14-0128.1.

[4] I. Lozovatsky and H. J. Fernando 2013 *Mixing efficiency in natural flows*, Philos. Trans. R. Soc. London, Ser. A **371**,(1982), 20,120,213.

[5] B. D. Mater and S. K. Venayagamoorthy 2014 *The quest for an unambiguous parameterization of mixing efficiency in stably stratified geophysical flows*, Geophysical Research Letters **DOI: 10.1002/2014GL060571**.

[6] L. H. Shih, J. R. Koseff, G. N. Ivey and J. H. Ferziger 2005 *Parameterization of turbulent fluxes and scales using homogeneous sheared stably stratified turbulence simulations*, Journal of Fluid Mechanics **525**, 193 – 214.

[7] H. Salehipour and W. R. Peltier 2015 *Diapycnal diffusivity, turbulent Prandtl number and mixing efficiency in Boussinesq stratified turbulence*, Journal of Fluid Mechanics **775**, 464 – 500.

Workshop on
Fundamental Aspects of Geophysical Turbulence II
at NCAR, 5-7 August 2015, Boulder, CO, USA

How far upscale does a dispersed phase influence turbulence?

David Richter[1] and Peter P. Sullivan[2]
[1]*Dept. of Civil and Environmental Engineering and Earth Sciences, University of Notre Dame, Notre Dame, Indiana 46556, U.S.A.*
[2]*National Center for Atmospheric Research, Boulder, Colorado 80307-3000, U.S.A.*

The turbulent suspension and transport of various types of dispersed phases occur frequently in nature, and take a wide variety of forms including sediment suspensions in water, dust/sand eroded from land, blowing snow, or water droplets in the form of cloud droplets, rain, or sea spray. In many circumstances these relatively small constituents are heavy and/or highly inertial, and are capable of modifying the flow in which they reside through both dynamic and thermodynamic couplings. This talk will focus primarily on the effects of momentum coupling between phases, and discuss the question of how far a particle's influence can be felt in high Reynolds number turbulence in both physical and spectral space.

Particle-laden turbulence has been studied extensively in many different contexts, particularly in the engineering community, and the so-called effect of "turbulence modulation", where the dispersed phase can either enhance or suppress turbulent kinetic energy, is well-documented in the literature [1]. The quantitative characteristics of this process are dependent on a number of factors including flow configuration, particle size, dispersed phase loading, etc., and a general description does not yet exist. In geophysical contexts, however, this turbulence modulation processes can play a critical role. For instance turbidity currents are entirely driven by the dispersed phase, and are self-limited due to turbulence suppression causing a cessation of sediment resuspension. Another example includes sea spray, which has been conjectured as a major factor in altering air-sea momentum and heat fluxes by modifying turbulence immediately above the ocean surface.

One of the key characteristics of geophysical turbulence is the very high Reynolds numbers that develop, which is indicative of the large scale separation that exists in these flows. At the same time, individual elements of commonly occurring dispersed phases (e.g., droplets, sand, etc.) are typically smaller than the smallest scales of turbulence in the atmosphere and ocean, and thus a natural question emerges: at what scale do turbulent motions in the environment stop being influenced by small dispersed phase constituents? A simple answer may be that these particles and droplets merely interact with motions similar to their own size — i.e., the dissipative motions. A more complex answer, one on which the present investigation focuses, is that particles can not only act directly on large scales through the formation of clusters, but that they also may induce an upscale information transfer by disrupting turbulence regeneration mechanisms.

To study this question of turbulence modulation across disparate scales, direct numerical simulations (DNS) two-way coupled with Lagrangian point particles are utilized in turbulent planar Couette flow at several increasing Reynolds numbers (see figure 1a). To account for two-way momentum coupling, the carrier phase momentum conservation equation is modified with a particle source term F_i:

$$\frac{\partial u_i}{\partial t} + u_j \frac{\partial u_i}{\partial x_j} = -\frac{1}{\rho_f}\frac{\partial p}{\partial x_i} + \nu_f \frac{\partial^2 u_i}{\partial x_j^2} + \frac{1}{\rho_f} F_i, \tag{1}$$

where ρ_f is the fluid density and ν_f is the fluid kinematic viscosity. The particle source term F_i is computed by projecting and summing the momentum gained from particles residing within the volume associated with each grid node. Each particle trajectory is integrated in time by solving $F = ma$ considering only a Stokes drag force. Simulations are performed at friction Reynolds numbers of $Re_\tau \approx [120, 300, 900]$ which are done on grids of $[128, 256, 128]$, $[256, 512, 256]$, and $[512, 1024, 512]$ respectively, with particle numbers up to 1×10^8.

From the DNS solutions, several analyses are performed to probe how far upscale the particle exert their influence. Basic single-point statistics indicate that particles can significantly reduce wall-normal velocity

fluctuations as well as turbulent momentum fluxes, while enhancing the strength of streaks, and that these trends actually increase in magnitude with increasing Reynolds number. Beyond these statistics, conditional averages are used to understand the structure of momentum fluxes at the wall, as well as how they are modified with particles (see Richter & Sullivan 2014 [2] and figure 1c). It is found that these near-wall "hairpins" are weakened significantly with the addition of various sizes of particles, and that this may cause a disruption of the self-sustaining near-wall turbulence process near the wall — a potential upscale feature of dispersed phase modulation which may play an important role at geophysical scales.

To better understand the scales over which the turbulence is modified, turbulent kinetic energy (TKE) and spectra of the TKE budget terms are computed as well. While it is not always straightforward to identify the dispersed phase influence as "TKE attenuation" or "TKE enhancement", it is found that the particles significantly reduce turbulent production across all available scales in the flow (see figure 1b). This broadband reduction of TKE production hints that particles can directly interact with large scales, while the direct source of TKE due to the momentum source F_i is small in magnitude but a much more complex function of scale and particle inertia.

The details of these analyses will be discussed, as well as their potential implications on how far their presence can be felt in atmospheric or oceanic turbulence. Analogs and preliminary results regarding heat and moisture transfer will be introduced and discussed as well. Unfortunately, the answer to the question posed in the title cannot be answered definitively, but the findings hint at how large-scale multiphase processes can be parameterized in the context of large eddy simulation or Reynolds avereraged Navier Stokes models.

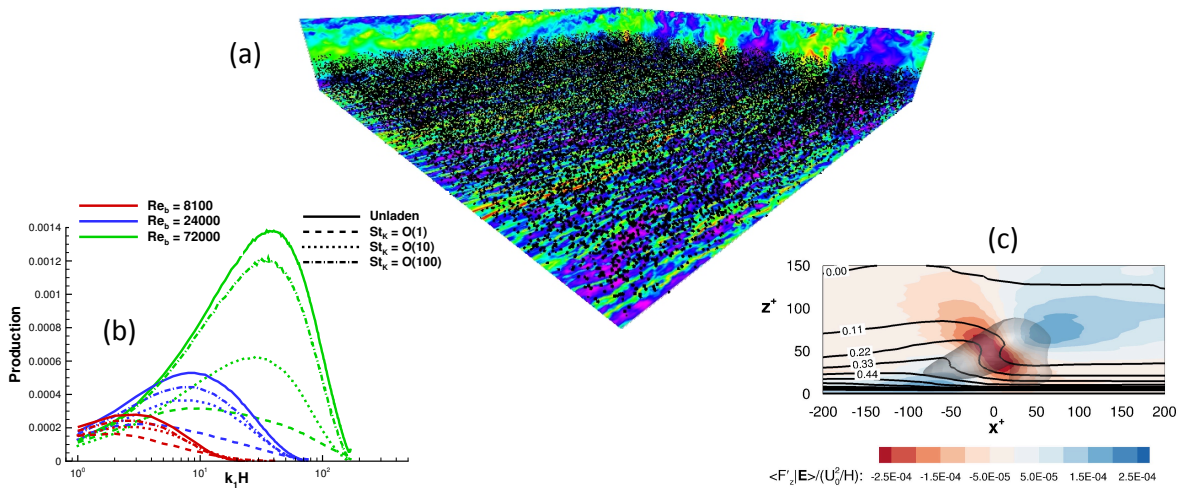

Figure 1: *(a) Instantaneous snapshot of particle-laden DNS. (b) TKE production spectra, illustrating the decrease in TKE production at all scales due to a dispersed phase, particularly at high Reynolds number. (c) Conditional near-wall eddy showing the weakening of momentum-flux-producing events at the wall.*

References

[1] S. Balachandar and J. Eaton 2010 *Turbulent dispersed multiphase flow*, Annual Review of Fluid Mechanics **42**, 111 – 133.

[2] D.H. Richter and P.P. Sullivan 2014 *Modification of near-wall coherent structures by inertial particles*, Physics of Fluids **26** 103304

[3] D.H. Richter 2015 *Turbulence modification by inertial particles and its influence on the spectral energy budget in planar Couette flow*, Physics of Fluids **27** 063304

Abstract for NCAR GTP Workshop, August 2015

Planetary Dynamos Driven by Helical Waves

P.A. Davidson

Dept. Engineering, University of Cambridge, Trumpington Street, Cambridge, UK.

Email: pad3@eng.cam.ac.uk

One of the most striking features of recent numerical simulations of planetary dynamos is that, despite being in the wrong parameter regime, they can produce magnetic fields that often look rather planet-like. That is to say, despite being overly viscous by a factor of around 10^9 (as measured by the Ekman number) and underpowered (relative to the onset of convection) by a factor of at least 100, many simulations produce sustained magnetic fields which are roughly dipolar outside the core and more or less aligned with the rotation axis, $\boldsymbol{\Omega}$, (see, e,g, Christensen, 2011). It is natural to ask, therefore, what underlying mechanisms might be at work in the simulations to produce quasi-steady dipolar magnetic fields aligned with $\boldsymbol{\Omega}$, and whether or not the same mechanisms might operate within the Earth, or indeed within the gas giants.

A tentative picture has emerged from these numerical simulations in which the dynamo action takes place mostly outside the tangent cylinder, an imaginary cylinder that circumscribes the solid inner core. Here the flow is seen to consist of thin columnar vortices aligned with the rotation axis, often in the form of alternating cyclones and anticyclones. These columnar vortices are observed to have a helical flow structure, with a helicity, $h = \mathbf{u} \cdot \nabla \times \mathbf{u}$, which is negative in the north (left handed spirals) and positive in the south (right-handed spirals). The dynamo is thought to be driven by these columnar vortices and indeed it is well known that such an asymmetric helicity distribution can support an α^2-dynamo. Since there is little evidence of a strong Ω-effect outside the tangent cylinder, it has become conventional to construe these numerical dynamos as of the α^2 type, located outside the tangent cylinder, and driven by helical motion within the columnar vortices.

As noted in Davidson (2014), one of the mysteries of this dynamo cartoon is the origin of the helicity, which is observed to be positive in the south and negative in the north. While Ekman pumping at the mantle can induce helicity in some of the overly viscous numerical

simulations, it is extremely unlikely to be a significant source within planets. In this talk we return to the suggestion of Davidson (2014, 2015) that the helicity observed in the less viscous simulations owes its existence to helical wave packets, launched in and around the equatorial plane where the buoyancy flux is observed to be strong. Here we show that such wave packets act as a potent source of planetary helicity, constituting a simple, robust mechanism that yields the correct sign for h north and south of the equator. Since such a mechanism does not rely on the presence of a mantle, it can operate within both the Earth and the gas giants. Moreover, our numerical simulations show that helical wave packets dispersing from the equator produce a random sea of thin, columnar cyclone/anticyclone pairs, very like those observed in the more strongly forced dynamo simulations.

We also examine the local dynamics of helical wave packets dispersing from the equatorial regions, as well as the overall nature of an α^2-dynamo driven by such wave packets. Our local analysis predicts the mean emf induced by the helical waves, while our global analysis yields exact integral relationships between the mean emf induced by the wave packets and the large-scale dipole and azimuthal field. Combining these local and integral equations yields a kinematic model for an α^2-dynamo driven by helical waves. Order-of-magnitude estimates based on these equations suggest that such a dynamo is indeed feasible.

References

Davidson, P. A. & Ranjan, A., 2015, Planetary Dynamos Driven by Helical Waves: Part 2, *Geophys. J Int.*, **202**, 1646-1662.

Davidson, P. A., 2014, The dynamics and scaling laws of planetary dynamos driven by inertial waves, *Geophys. J Int.*, **198** (3), 1832-1847.

Workshop on
Fundamental Aspects of Geophysical Turbulence II
at NCAR, 5-7 August 2015, Boulder, CO, USA

Turbulence and waves on a westward jet - an experimental study

Boris Galperin[1], Jesse Hoemann[1], Stefania Espa[2], Guglielmo Lacorata[3], Gabriella Di Nitto[2]
[1] *College of Marine Science, University of South Florida, St. Petersburg, Florida, U.S.A.*
[2] *DICEA, Sapienza Università di Roma, Via Eudossiana 18, 00184 Rome, Italy*
[3] *ISAC, National Research Council, Str. Prov. Lecce-Monteroni, 73100 Lecce, Italy*

Fundamental Aspects of Geophysical Turbulence II
at NCAR, 5-7 August 2015, Boulder, CO, USA.

Extended abstract

The role of powerful eastward jets in geophysical flows is well known. The westward jets have received a relatively lesser attention although their role is also prominent. A few examples are β-plumes in the oceans, the South-Equatorial Currents in the Atlantic and Pacific Oceans that produce the Tropical Instability Waves (TIW), and the jet that spins off the String of Pearls on Saturn. All these systems feature Rossby waves. In addition, they are seasonally forced, become unstable and produce westward propagating eddies. The signature of these eddies has been well observed and they are known to affect circulations and climates. The dynamics of such systems is not well understood. Their large-scale turbulence (i.e., macroturbulence) often involves anisotropic inverse energy cascade which is difficult to diagnose and quantify. A simple diagnostic tool for such systems could significantly advance their understanding and modeling.

Here, we report on experimental investigation of westward jets featuring turbulence with inverse energy cascade. Turbulence and the jet were produced by an electro-magnetic force in a rotating tank filled with an electrolytic saline solution. The parabolic free surface emulated the topographic β-effect which evoked the zonation. The working area included one forced and three unforced sectors such that forced and unforced flows, as well as their combination could be studied.

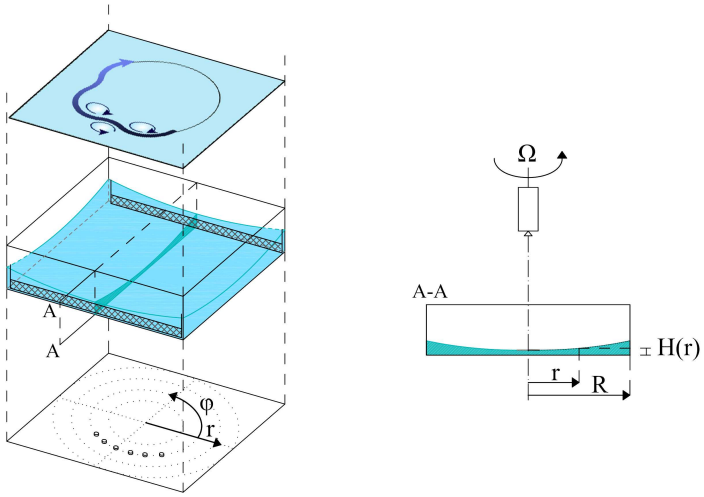

Figure 1: *Schematic representation of the experimental device. The magnets are placed in a 90° arc of the radius a = 17 cm (sector I).*

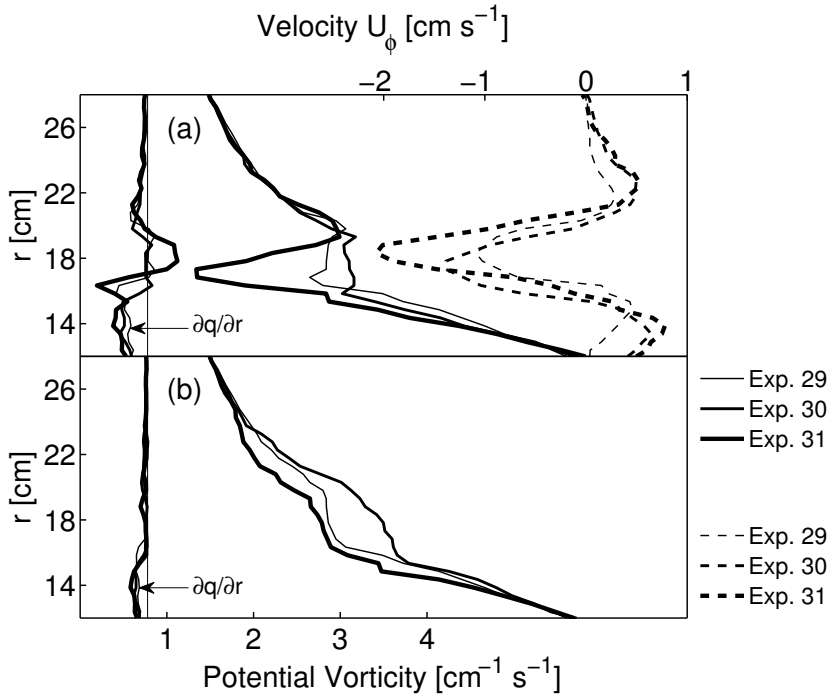

Figure 2: Top: snapshots of the azimuthal velocity, U_ϕ (dashed lines), and corresponding potential vorticity, q (solid lines). Profiles on the left are $\frac{\partial q}{\partial r}$. The vertical line corresponds to $\frac{\partial q}{\partial r} = 0$. The instantaneous velocity profiles are barotropically unstable most of the time. Bottom: PV and $\frac{\partial q}{\partial r}$ profiles after monotonizing.

The spectral and transport flow characteristics of the resulting flows were highly anisotropic. To diagnose turbulence, we extended the analogy with the Phillips' effect and explored the connection between turbulent overturns in stably stratified and quasi-geostrophic flows and developed a novel method based upon the *monotonizing of potential vorticity* (PV). The mean displacement from the Thorpe-monotonized PV profile yields a length scale, L_M, analogous to the Thorpe's scale used in flows with stable stratification. As the Thorpe scale is proportional to the Ozmidov scale, the scale L_M is proportional to the scale $L_\beta = (\epsilon/\beta^3)^{1/5}$ at which the turbulence eddy turnover time is commensurable with the Rossby wave period.
Figure 2 displays sample profiles of instantaneous azimuthal velocity, corresponding PV and respective monotonized PV using the Thorpe's sorting algorithm. Throughout the experiments, the jets are barotropically unstable. The non-monotonousness of PV increases with increasing forcing due to growing turbulent overturns. On the other hand, PV monotonizing renders all profiles stable as it "flushes out" turbulence.

The anisotropization of transport properties of the flow is investigated using the finite scale Lyapunov exponent (FSLE) technique. After initial exponential particle separation, diffusion obeys the Richardson law in both azimuthal and radial (zonal and meridional) directions. On larger scales, the radial diffusion attains the Taylor (scale-independent diffusivity) regime while the azimuthal diffusion continues to follow the Richardson law. The transition to the Taylor regime for the radial diffusion takes place at a scale of turbulence anisotropization. The azimuthal and radial eddy diffusivities in both regimes as well as the transition scale are all determined by the rate of the inverse energy cascade, ϵ, that can be diagnosed by the PV monotonizing. Conversely, ϵ can be deduced from the scale of the Richardson-Taylor transition in the radial eddy diffusivity which, thus, provides an additional tool of diagnosing anisotropic turbulence with inverse energy cascade. The advantages of these methods are in that they can be applied locally while not relying upon data intense spectral analysis.

Workshop on
Fundamental Aspects of Geophysical Turbulence II
at NCAR, 5-7 August 2015, Boulder, CO, USA

The diurnal cycle of the ocean surface boundary layer

S.E. Belcher[1,2], A.L.M. Grant[2], B.C. Pearson[2], J.A. Polton[3], M.R. Palmer[3], N. Lucas[4], T. Rippeth[4], G. Damerell[5], K.J. Heywood[5] and the OSMOSIS consortium
[1]*Met Office Hadley Centre, Met Office, Exeter, UK*
[2]*Department of Meteorology, University of Reading, Reading, UK*
[3]*National Oceanography Centre, UK*
[4]*School of Ocean Sciences, University of Bangor, Bangor, UK*
[5]*School of Environmental Science, University of East Anglia, UK*

The ocean surface boundary layer (OSBL), typically of depth 10-100m, is a turbulent layer that couples the ocean to the atmosphere. Over the past 20 years it has become increasingly apparent that the turbulence in the OSBL is strongly affected by the surface waves that propagate on the atmosphere–ocean interface. There are four distinct mechanisms whereby surface waves interact with the OSBL (see [1] for a review). Firstly, breaking surface waves inject turbulence into the water [2]. Secondly, straining motions associated with the surface waves strongly modulate the turbulence through a wavelength of the wave [3]. Thirdly, the rectified Stokes drift associated with the waves leads to a vortex force that deforms vorticity the water flow [4]. Fourthly, the interaction of the Stokes drift with the planetary rotation yields a Coriolis-Stokes force on the mean flow [5]. Together these processes render the OSBL a quite different turbulent layer when compared with the atmospheric boundary layer. New parameterisations are therefore required for global climate models in order to account for these processes.

In this talk the focus will be on the third process, namely the effect of the Stokes drift on turbulence in the OSBL, which generates *Langmuir Turbulence* [6], an asymptotically distinct type of turbulence with its own scaling laws [7]. The scaling laws indicate that deepening of the OSBL by Langmuir turbulence is more rapid than by pure shear turbulence, because the Langmuir turbulence organises more of the turbulent kinetic energy into vertical motion [7, 8]. Langmuir turbulence has been shown to be likely to be the dominant form of turbulence in the global oceans, and so could lead to deeper OSBL which would correct biases in many global models [9]. Here we present new measurements of the turbulence in the upper ocean, which we interpret using Large Eddy Simulations and theory to demonstrate how Langmuir turbulence controls the diurnal cycle of the OSBL.

New observations of the turbulent dissipation rate in the upper ocean were made during the OSMOSIS cruise in the N.E. Atlantic in September 2012. The measurements were made using a turbulence probe mounted on an ocean glider that was deployed during the cruise. The turbulence dissipation rate provides a particularly sensitive measure of the turbulence in the OSBL and demonstrates that during periods of relatively low wind the OSBL exhibits a strong diurnal cycle. During the night the OSBL is driven at the surface by a combination of cooling and wind-wave forcing leading to a combination of convective and Langmuir turbulence, which deepens the OSBL. After sunrise, solar radiation warms the water column over the finite depth over which the radiation is absorbed by the water. The absorption of radiation after sunrise varies with depth and the turbulence must do work against the stable stratification that is produced. In pure wind forcing, in the absence of the wave effects, the layer would form a stably stratified shear layer with a strong temperature gradient near the surface (as in the nocturnal atmospheric boundary layer). The wind-wave forcing, however, continues to drive mixing via Langmuir turbulence, leading to a shallow well mixed layer overlying a diurnal thermocline (as also seen by [10]). Observations of the temperature profile indicate the presence of a well mixed layer, consistent with Langmuir turbulence.

We perform Large Eddy Simulations of an idealised diurnal cycle, which capture this diurnal cycle well when the effects of Langmuir turbulence are included [11]. More realistic simulations forced by the observed surface fluxes indicate that the LES, which accounts for the Langmuir turbulence via the vortex force, quantitatively captures the structure of the turbulence measured during the cruise.

As a first step towards developing a parameterisation of these processes suitable for global climate models, a prognostic equation for the depth of the OSBL is developed based on scaling laws developed using the LES data. The prognostic equation accounts for deepening by convection and Langmuir turbulence and by shoaling due to solar heating and is based on conservation of heat, mean potential energy and turbulent kinetic energy in the layer. The prognostic equation reduces to the standard mixed layer model in purely convective conditions. The model agrees well with the measurements over the course of the cruise period, including several pronounced diurnal cycles and a period of sustained deepening through wind-wave forcing. Long term measurements of the OSBL from sea gliders during the OSMOSIS long-term measurement campaign track the evolution of the depth of the OSBL over a whole year. Initial results indicate that the prognostic equation for the depth of the layer captures the evolution well, without the need for tuning. By correctly accounting for Langmuir turbulence, the model reproduces extended periods of deepening of the OSBL. If Langmuir turbulence is not represented then the deepening of the layer is too slow.

This work provides compelling evidence that Langmuir turbulence plays a pronounced role in shaping the evolution of the OSBL. The prognostic equation of the depth of the OSBL is one of the building blocks for a parameterisation of the OSBL that can account for these processes in global climate models.

References

[1] P.P. Sullivan and J.C. McWilliams 2010 *Dynamics of Winds and Currents Coupled to Surface Waves*, Ann. Re. Fluid Mech. **42**, 19 – 42.

[2] E.A. Terray, M.A. Donelan, Y.C. Agrawal, W.M. Drennan, K.K. Kahma, A.J. Williams, P.A. Hwang and S.A. Kitaigorodskii *Estimates of kinetic energy dissipation under breaking waves* J. Phys. Oceanogr. **26** 792 – 807.

[3] M.A.C. Teixeira and S.E. Belcher 2002 *On the distortion of turbulence by a progressive surface wave.* J. Fluid Mech. **458** 229 - 267.

[4] A. Craik and S. Leibovich 1976 *A rational model for Langmuir circulations.* J. Fluid Mech. **73** 401 - 426.

[5] J.A. Polton, D.M. Lewis and S.E. Belcher 2005 *The role of wave-induced Coriolis-Stokes forcing on the wind-driven mixed layer.* J. Phys. Oceanogr. **35** 444 - 457

[6] J.C. McWilliams, P.P. Sullivan and C.H. Moeng 1997 *Langmuir turbulence in the ocean.* J. Fluid Mech. **334** 1 - 30

[7] A.L.M. Grant and S.E. Belcher 2009 *Characteristics of Langmuir turbulence in the ocean mixed layer.* J. Phys. Oceanogr. **39** 1871 – 1887

[8] J.A. Polton and S. E. Belcher 2007 *Langmuir turbulence and deeply penetrating jets in an unstratified mixed layer* J. Geophys. Res. **112** C09020, doi:10.1029/2007JC004205.

[9] S.E. Belcher and others 2012 *A global perspective on mixing in the ocean surface boundary layer.* Geophys. Res. Lett. **39** L18605, doi:10.1029/2012GL052932

[10] T. Kukulka, A. J. Plueddemann and P. P. Sullivan 2013 *Inhibited upper ocean restratification in nonequilibrium swell conditions* Geophys. Res. Lett. **40** 15, doi:10.1002/grl.50708

[11] B.C. Pearson, A.L.M. Grant, J.A. Polton and S.E. Belcher 2015 *Langmuir Turbulence and Surface Heating in the Ocean Surface Boundary Layer* J. Phys. Oceanogr. *In Press*

Workshop on
Fundamental Aspects of Geophysical Turbulence II
at NCAR, 5-7 August 2015, Boulder, CO, USA

Synchronization of Chaos in Fully Developed Turbulence

Cristian C. Lalescu[1,2], Charles Meneveau[3] and Gregory L. Eyink[1]
[1] *Department of Applied Mathematics and Statistics, Johns Hopkins University, Baltimore, U.S.A.*
[2] *Current address: Max Planck Institut, Goettingen, GERMANY*
[3] *Department of Mechanical Engineering and Institute for Data Intensive Engineering and Science (IDIES), Johns Hopkins University, Baltimore, U.S.A* (presenter).

Motivated by fundamental questions about chaotic dynamics in multiscale systems governed by nonlinear PDE's, we consider the feasibility of reproducing actual instantaneous realizations based on coarse-grained numerical simulations. The relevant framework is chaos synchronization, where one is interested in dynamical slavings that may develop among various sets of degrees of freedom comprising a nonlinear dynamical system. Relevant to turbulent flow here we consider the case of Navier-Stokes turbulence. We investigate chaos synchronization of small-scale motions in the three-dimensional turbulent energy cascade, via pseudospectral simulations of the incompressible Navier-Stokes equations. The modes of the turbulent velocity field below about 20 Kolmogorov dissipation lengths are found to be slaved to the chaotic dynamics of larger-scale modes. The dynamics of all dissipation-range modes can be recovered to full numerical precision by solving small-scale dynamical equations with the given large-scale solution as an input, regardless of initial condition. The synchronization rate exponent scales with the Kolmogorov dissipation time scale, with possible weak corrections due to intermittency.

Figure 1, reproduced from Lalescu *et al.* [1], shows the exponential rate at which a partially resolved simulation converges toward a fully resolved simulation, for various levels of coarse-graining (cut-off wavenumber). Everything is scaled in Kolmogorov units. The rate is negative (convergence) up to some threshold wavenumber (corresponding approximately to $k_c\eta_K \sim 0.2$) below which, at coarser resolution, individual realizations diverge exponentially from the finely resolved dynamics, with positive exponential rate. Our results suggest that all sub-Kolmogorov length modes should be fully recoverable from numerical simulations with standard, Kolmogorov-length grid resolutions. It is of interest, especially for geophysical applications, to clarify how

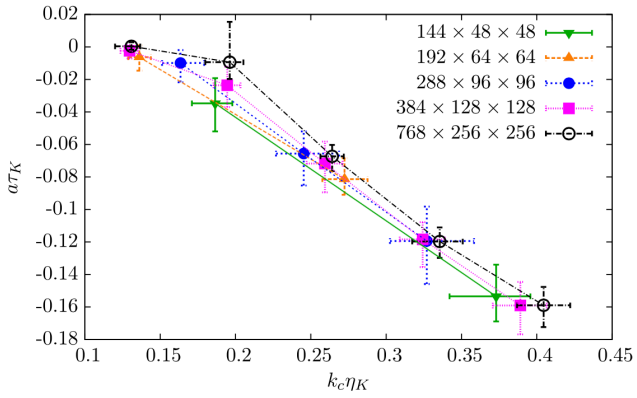

Figure 1: *Symbols: average of synchronization exponents as a function of the cutoff wave number for five different simulation sizes and Reynolds numbers, plotted in Kolmogorov units. Error bars are for maximum and minimum values of different runs and ranges used in the fit.*

this result can be reconciled with and is distinct from the Kraichnan-Leith theory [2] on inverse cascade of errors in a turbulent flow. Our formulation "freezes" the dynamics of the low wave numbers and only allows multiple realizations of the high wavenumbers to evolve. This is in contrast to the "error field" (difference of two NS solutions) discussed by Kraichnan-Leith, which involves all wavenumbers.

The presentation will thus summarize the findings of Lalescu *et al.*[1] and will also provide an overview of the Turbulence Numerical Laboratory [3, 4, 5], where several Direct Numerical Simulation (DNS) Databases of various turbulent flows are available for public access. The feasibility of 'resimulation' of coarsely stored DNS data is discussed in light of the insights gained about synchronization of chaos in turbulent flows.

This work is supported by the National Science Foundations CDI-II program, Project No. CMMI-0941530, with additional support through Grant No. NSF-OCI-108849.

References

[1] C.C. Lalescu, C. Meneveau and G.L. Eyink (2013), *Synchronization of Chaos in Fully Developed Turbulence*, Phys. Rev. Letts. **110**, 084102.

[2] C. E. Leith and R. H. Kraichnan (1972), *Predictability of turbulent flows*, J. Atmos. Sci. **29**, 1041.

[3] Y. Li, E. Perlman, M. Wan, Y. Yang, C. Meneveau, R. Burns, S. Chen, A. Szalay and G.L. Eyink (2008), *A public turbulence database cluster and applications to study Lagrangian evolution of velocity increments in turbulence*, J. Turbulence **9**, No. 31.

[4] H. Yu, K. Kanov, E. Perlman, J. Graham, E. Frederix, R. Burns, A.Szalay, G.L. Eyink and C. Meneveau (2012), *Studying Lagrangian dynamics of turbulence using on-demand fluid particle tracking in a public turbulence database*, J. Turbulence **13**, No. 12.

[5] J. Graham, K. Kanov, X.I.A. Yang, M. K.Lee, N. Malaya, C.C. Lalescu, R. Burns, G. Eyink, A. Szalay, R.D. Moser, and C. Meneveau (2015), *A Web Services-accessible database of turbulent channel flow and its use for testing a new integral wall model for LES*, J. Turbulence (submitted).

Workshop on
Fundamental Aspects of Geophysical Turbulence II
at NCAR, 5-7 August 2015, Boulder, CO, USA

The prediction horizon of convective boundary layers

Harmen Jonker, Siddhartha Mukherjee and Jerôme Schalkwijk
Department of Geoscience and Remote Sensing, Delft University of Technology, NETHERLANDS

The fundamental predictability horizon of convective boundary layers is investigated in this study. Large-eddy simulation (LES) and direct numerical simulation (DNS) techniques are employed to probe the evolution of perturbations in identical twin simulations of a growing dry convective boundary layer. We confine ourselves to the W06 case of [2], a CBL capped by a weak inversion jump. Error propagation is studied by performing identical twin simulations. The simulations are allowed to evolve for a one hour spin-up period, after which one of them is perturbed. The perturbations employed in this study are two dimensional sinusoidal fields added to the potential temperature field, and have a fixed amplitude δ_0 and (dimensionless) wavenumber k_p in the x and y directions:

$$\theta_2 = \theta_1 + \delta_0 \sin\left(2\pi k_p \frac{x}{L}\right) \sin\left(2\pi k_p \frac{y}{L}\right) \tag{1}$$

where θ_1 and θ_2 are the potential temperature fields of the two separate (twin) simulations just after perturbation. The evolution of the perturbation is reported as a slab averaged root mean square difference between the potential temperature fields in two simulations, given as

$$\delta(t) = \sqrt{\langle(\theta_1 - \theta_2)^2\rangle} \tag{2}$$

where the brackets $\langle\rangle$ denote a volume average. The perturbation energy spectrum is calculated from the Fourier decompositions of the potential temperature difference $(\theta_1 - \theta_2)$ in the two horizontal directions. The spectra are further averaged over the vertical direction.

The top panel of Figure 1 shows the evolution of $\delta(t)$, the volumetric error evolution after a perturbation given in (1), for $\Delta x = \Delta y = 12.5$ m and $\Delta z = 10$ m, with the perturbation wavenumber varying from $k_p = 4$ to 36 (corresponding to wavelengths between 100 m and 1 km). After the initial phase, the error evolution displays a well-behaved exponential growth rate, which can be approximated as

$$\delta(t) \approx \delta_0 e^{\Lambda t} \tag{3}$$

where Λ is the Lyapunov exponent.

The constant exponential growth phase in Figure 1(top) shows the Lyapunov exponent to be independent of the perturbation wavenumber. This indicates a rapid redistribution of the error spectrum after seeding, after which a self similar spectral shape governs the growth of error. The initial decrease in the error (see inset) is steeper for higher wavenumbers indicating that small scale errors decrease more significantly than large scale errors. This is related to dissipation by the subgrid model, which acts more strongly on sharper gradients encountered for higher wavenumbers.

The evolution of the error field is shown as a vertical slice in the middle of the domain in Figure 1 (middle panel) for the case of $k_p = 4$ for the four intervals marked on the error-growth curve in the top panel. The corresponding vertically averaged 2D power spectra of the error field are shown below. Interval (a) shows the error seed, which peaks at a single wavenumber, and is seen to immediately interact with all other scales which begin to grow as seen from the upward shifting power spectrum. Interval (b) shows the error during the constant exponential growth phase following $\delta(t) \approx \delta_0 e^{\Lambda t}$. Note that the shape of the power spectrum in this phase is self similar and is dominated by the higher wavenumbers. It continually shifts upward with an equal distance (on a log scale) reflecting the constant growth rate. This feature is observed for all the

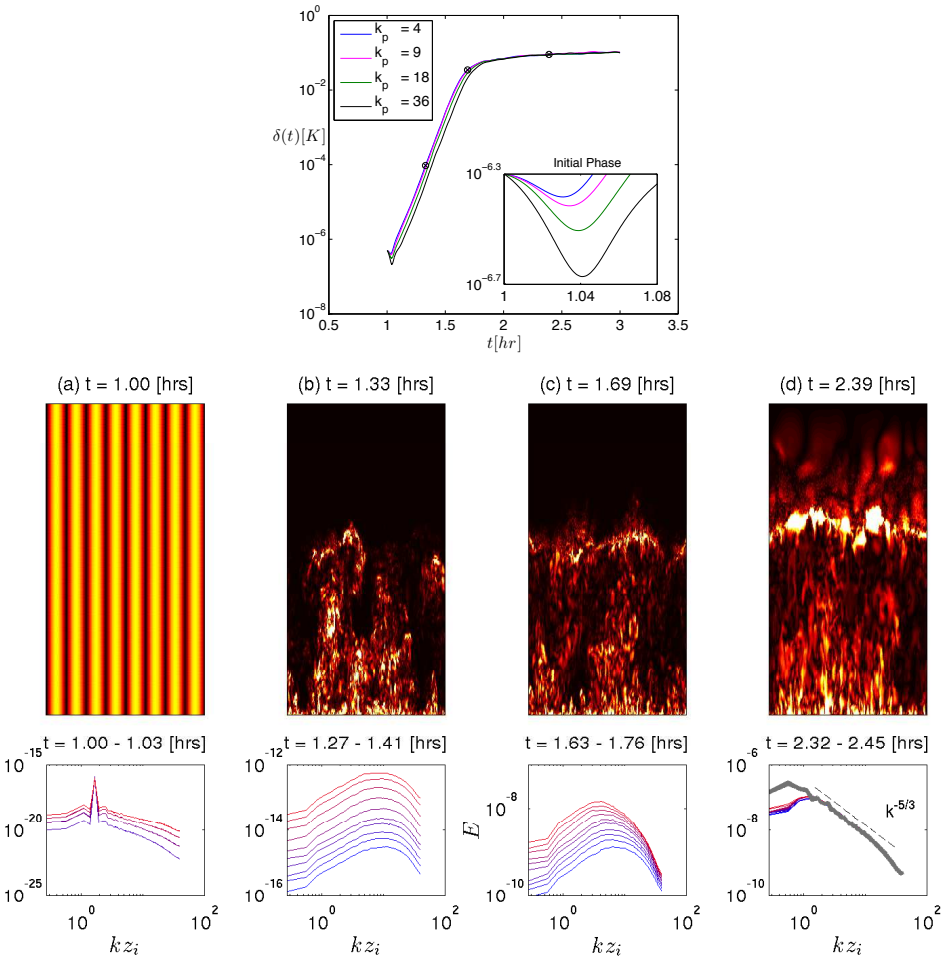

Figure 1: Top: Volumetric error growth for different perturbation wavenumbers k_p. Middle: cross sections of the error field for the 4 instances marked on the error curve in top panel. Bottom: corresponding error power spectra.

simulations performed in this study; (c) shows the transition to saturation of the error energy in which the larger scales begin to saturate at a slower rate; (d) shows the fully saturated phase of the error.

Furthermore, it is found that the error growth rates display a strong dependence on the Reynolds number. A detailed analysis of the decorrelation times per individual scale reveals two regimes: a Re independent regime for scales larger than the boundary layer height z_i and a Re dependent regime for scales smaller than z_i, which are found to decorrelate substantially faster for increasing Reynolds numbers. Implications for realistic convective atmospheric boundary layers are discussed.

References

[1] E. Lorenz 1969 *The predictability of a flow which possesses many scales of motion,* Tellus, **21** 289–307.

[2] P. Sullivan, C-H Moeng, B. Stevens, D. Lenschow, and S. Mayor 1998 *Structure of the entrainment zone capping the convective tmospheric boundary layer,* Journal of the Atmospheric Sciences, **55** 3042–3064.

Workshop on
Fundamental Aspects of Geophysical Turbulence II
at NCAR, 5-7 August 2015, Boulder, CO, USA

Co-spectral budgets link energy distributions in eddies to bulk flow properties

Gabriel Katul[1], Costantino Manes[2], Elie Bou-Zeid[3], Marcelo Chamecki[4], Dan Li[5], and Charles Meneveau[6]

[1]*Nicholas School of the Environment, Duke University, Durham, NC 27708-0328, U.S.A.*
[2]*Faculty of Engineering and the Environment, University of Southampton, Southampton, United Kingdom*
[3]*Department of Civil and Environmental Engineering, Princeton University, Princeton, NJ08544, U.S.A.*
[4]*Department of Meteorology, the Pennsylvania State University, University Park, PA 16802-501*
[5]*Program of Atmospheric and Oceanic Sciences, Princeton University, Princeton, NJ08544, U.S.A.*
[6]*Department of Mechanical Engineering, Johns Hopkins University, Baltimore, MD 21218, U.S.A.*

Among the most important phenomenological theories of turbulence in the atmospheric surface layer, two are often singled out: (i) the von Kármán-Prandtl logarithmic law for the mean velocity profile $U(z)$ adjusted by stability correction functions as proposed by Monin and Obukhov surface layer similarity, and (ii) the Kolmogorov hypothesis (hereafter referred to as K41) for the local structure of the turbulent velocity. These developments have often been regarded as separate given that the *log-law* is presumed to be an outcome of restrictive boundary effects on eddy sizes responsible for mixing, while the local structure of turbulence is associated with locally homogeneous and isotropic turbulence far from any boundary. Furthermore, these theories have stirred significant debate and continue to receive attention and novel interpretations [1]. Intermittency corrections to the local structure of turbulence modify the $-5/3$ spectral exponent by α that is linked to the well-known intermittency parameter μ (e.g. $\alpha = -\mu/9$ in the log-normal model), and laws other than logarithmic have been routinely used to represent $U(z)$ in the absence of any stratification. Over the past two decades, connections between these two theories were explored using incomplete similarity and intermediate asymptotics [2] and through the so-called 'spectral link' [1] in the absence of thermal stratification. Here, a phenomenological theory that builds on these previous connections is proposed using a co-spectral budget for the turbulent stress normal to the wall [3]. It is shown that the co-spectral budget (i) is consistent with the onset of a $-7/3$ power-law scaling in the co-spectrum between longitudinal and normal velocity fluctuations for eddies within the inertial subrange associated with K41, (ii) leads to novel linkages among phenomenological and model closure constants, (iii) provides a new perspective on linkages between intermittency corrections to K41 within the inertial subrange (e.g. $\mu > 0$) and the onset of logarithmic or power-law mean velocity profiles in the neutral surface layer, and (iv) accommodates thermal stratification leading to the stability correction functions. Depending on the choices made about how small-scale intermittency corrections are introduced into the energy cascade, logarithmic or power-law $U(z)$ emerge with an exponent that depends on μ given by

$$\frac{dU}{dz} = \frac{u_*}{z}\left(\frac{A}{C'_K}\frac{3-4\alpha}{7-3\alpha}\right)^{3/4}\left(\frac{z}{L_o}\right)^{3\alpha/4}. \tag{1}$$

Here, u_* is the friction velocity, z is the height from the boundary, L_o is a length scale at the cross-over from production to inertial subrange scales, A is the Rotta constant, and C'_K is the Kolmogorov constant for the vertical velocity spectrum in 1-D. According to the solution of the co-spectral budget, Log-laws in $U(z)$ prevail when $\mu = 0$ or, alternatively, when $L_o = z$ as may be expected for the vertical velocity energy spectrum.

The co-spectral budget is then generalized to include the effects of thermal stratification using a Richardson number so as to predict the mixing efficiency associated with eddy diffusivity for heat, or equivalently

the turbulent Prandtl number (Pr_t). The focus here is on stably stratified surface layer flows given that such flows are fraught with complex dynamics originating from scale-wise interplay between shear generation of turbulence and its dissipation by density gradients. Yet, despite this flow complexity, a large corpus of data and numerical simulations agree on a near-universal relation between Pr_t and the gradient Richardson number (R_g), which encodes the relative importance of buoyancy dissipation to mechanical production of turbulent kinetic energy. This quasi-universal $Pr_t - R_g$ relation, shown in Figure 1, is also derived from the aforementioned co-spectral budgets for momentum amended to include heat fluxes [4]. It is shown that the ratio of C'_K to the Kolmogorov-Obukhov-Corrsin (C_T) phenomenological constant for the temperature spectrum, and a constant C_{IT} associated with isotropization of the production whose value (= 3/5) has been predicted from Rapid Distortion Theory, explain all the macroscopic nonlinearities in the $Pr_t - R_g$ relation shown in Figure 1 and is given by

$$Pr_t^{-1} = \frac{1}{2R_g}\left[1 + \omega_2 R_g - \sqrt{-4R_g + (-1 - \omega_2 R_g)^2}\right], \tag{2}$$

where $\omega_2 = 1 + \omega_1$, and $\omega_1 = (1 - C_{IT})^{-1} C_T (C'_K)^{-1}$. Hence, it may be conjectured that much of the universal character of bulk flow properties in surface layer turbulence, often predicted from similarity theories or dimensional considerations, appears to be inherited from the phenomenological theory of turbulence describing the kinetic and thermal energetics of eddies.

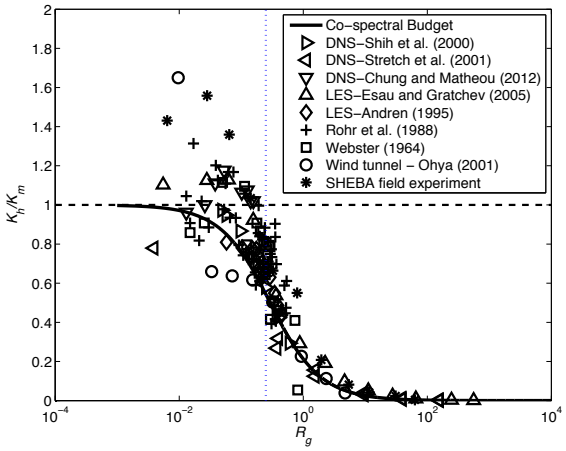

Figure 1: *The relation between the inverse turbulent Prandtl number (Pr_t^{-1}) defined by the ratio of turbulent diffusivities for heat K_h and momentum K_m and the gradient Richardson number R_g. Predictions from the co-spectral budget are also shown.*

References

[1] G. Gioia, N. Guttenberg, N. Goldenfeld, and P. Chakraborty 2010 *Spectral theory of the turbulent mean-velocity profile*, Physical Review Letters **105**, 184501.

[2] G.I. Barenblatt, and A. J. Chorin 1998 *New perspectives in turbulence: Scaling laws, asymptotics, and intermittency*, SIAM review **40**, 265–291.

[3] G.G. Katul, A. Porporato, C. Manes, and C. Meneveau 2013 *Co-spectrum and mean velocity in turbulent boundary layers* Physics of Fluids **40**, 091702

[4] G.G. Katul, A. Porporato, S. Shah, and E. Bou-Zeid 2014 *Two phenomenological constants explain similarity laws in stably stratified turbulence* Physical Review E **89**, 023007

Workshop on
Fundamental Aspects of Geophysical Turbulence II
at NCAR, 5-7 August 2015, Boulder, CO, USA

Canopy-Boundary Layer Coupling in Convectively Unstable Flows: A Tale of Interacting Instabilities

John J. Finnigan[1], Edward G. Patton[2], Roger H. Shaw[3]
[1] *CSIRO Oceans and Atmosphere, Canberra, Australia*
[2] *National Center for Atmospheric Research, Boulder, Colorado, U.S.A.*
[3] *University California Davis, Davis, California, U.S.A.*

The origin of the coherent eddy structures in and above tall plant canopies in neutrally stratified flow has been known for some years to result from the hydrodynamic instability of the inflected mean velocity profile that develops at the canopy top. A cascade of secondary instabilities yields canopy eddies of characteristic form and these are responsible for most of the turbulent kinetic energy and transport in the canopy's vicinity.

Above the surface layer, in neutral and weakly unstable flows, large-scale roll-like structures dominate transport throughout much of the larger atmospheric boundary layer (ABL). When buoyancy forces become dominant, these rolls transition into Rayleigh-Bénard-like cells spanning the depth of the convectively driven ABL. At the canopy level, these ABL-scale structures modulate the near-surface wind and temperature fields so that canopy regions are alternately subjected to enhanced or reduced wind shear and diabatic stability at horizontal scales ranging from 100-1000 canopy heights.

Beneath these ABL-scale structures in regions of strong shear, the canopy eddy structure corresponds to the inflection point instability described above. However in regions of low shear, diabatic effects dominate and convective plumes develop, extending vertically to several canopy heights and with horizontal widths of order canopy height. These canopy plumes are a mode of buoyant instability with Rayleigh-Bénard type eigenmodes, whose horizontal scale is related to the vertical profile of canopy air temperature.

The horizontally-averaged heat and momentum transfer between the canopy layers and the ABL above therefore results from two distinct coherent eddy structure types, according to whether the canopy is below ascending or descending regions of the larger ABL-scale structures. Because the structure of the large ABL-scale rolls or cells above the canopy depends upon the area-averaged heat and momentum transfer from the surface through the parameter z_i/L_{MO} (the ABL depth divided by the Obukhov length), these three modes of instability, two at canopy scale and one at ABL scale, are intimately coupled.

We have studied this situation using canopy-resolving large eddy simulations (LES) of the full ABL. In addition, we have complemented those full LES simulations with idealized studies of the canopy plume instability.

In this talk we will discuss the implications of this fully coupled picture of canopy-ABL turbulent exchange for Monin-Obukhov scaling in the surface and canopy-roughness sublayers, and for observational strategies for tower measurements of turbulent fluxes. We will also comment on the usefulness of linear and non-linear stability analysis in revealing attractors for dominant turbulence structures even in fully turbulent flows.

Workshop on
Fundamental Aspects of Geophysical Turbulence II
at NCAR, 5-7 August 2015, Boulder, CO, USA

Optical turbulence: from first principles to working models

Andreas Muschinski

NorthWest Research Associates, Inc., 3380 Mitchell Lane, Boulder, Colorado, U.S.A.

It has been known since Newton's times that small-scale temperature fluctuations in the turbulent atmosphere limit the performance of astronomical telescopes dramatically. However, there was relatively little first-principle understanding of stellar scintillation and related phenomena prior to the pioneering work by Tatarskii and his co-workers in the 1950s and 1960s [1, 2]. Tatarskii's theory of wave propagation through the turbulent atmosphere is built on first-principle hydrodynamics (the Navier-Stokes equations and the temperature transport equation); first-principle electromagnetics (Maxwell's equations); the mathematical theory of stochastic processes and random fields; and the semi-empirical Kolmogorov [3] and Obukhov-Corrsin [4, 5] similarity theories of turbulence in the velocity and temperature fields, respectively.

During the last 50 years, Tatarskii's theory has been enhanced and refined in response to scientific and technological needs in various areas, including optical remote sensing of the turbulent atmosphere, terrestrial and extraterrestrial imaging and surveillance, free-space optical communication, and directed energy; see, e.g., Refs. [6, 7, 8, 9].

The three-dimensional spectrum $\Phi(\boldsymbol{\kappa})$ of the turbulent air temperature fluctuations is a key quantity in the physics of optical propagation through the turbulent atmosphere. The standard model, which was derived in the 1950s by Tatarskii from the Obukhov-Corrsin theory of homogeneous and isotropic turbulence, is

$$\Phi(\kappa) = 0.033\, C_T^2 \kappa^{-11/3} h(\kappa l_0), \tag{1}$$

where $\kappa = |\boldsymbol{\kappa}|$ is the wave number, C_T^2 is the temperature structure parameter, l_0 is the inner temperature scale, and $h(\kappa l_0)$ is a universal function that approaches 1 for wave numbers in the inertial range and drops rapidly to zero for $\kappa l_0 > 1$. For Fresnel lengths comparable to l_0, certain performance characteristics of optical systems, such as the scintillation index, depend sensitively on the functional form of $h(\xi)$ at $\xi \approx 1$. During the last 70 years, the optical-turbulence community has developed and applied various heuristic $h(\xi)$ models.

Here I show that there is a first-principle constraint that any valid $h(\xi)$ model has to fulfill:

$$\int_0^\infty \xi^{1/3} h(\xi) d\xi = \frac{27\,\Gamma(1/3)}{10} = 7.233. \tag{2}$$

This constraint is a non-dimensional form of the temperature variance dissipation equation, which follows from first-principle fluid mechanics. We show that Tatarskii's cut-off (1961) and Gaussian (1971) models fulfill this constraint while three more recent $h(\xi)$ models, including the widely used Andrews (1992) model [10], do not; see Figures 1 and 2.

During the last ten years, the optical-propagation community has produced and applied models for the temperature spectrum in "non-Kolmogorov" turbulence; see, e.g., Ref. [11] and references cited therein. These models are not consistent with the Obukhov-Corrsin similarity theory. In particular, the power-law exponent of $\Phi(\kappa)$ in the low-wave-number regime is treated as a free parameter that may differ from the classical value $-11/3$. At present, it is unclear to what extent these models for "non-Kolmogorov" turbulence are consistent with first principles of fluid mechanics (such as the temperature variance dissipation equation) and with state-of-the-art in-situ measurements of atmospheric turbulence.

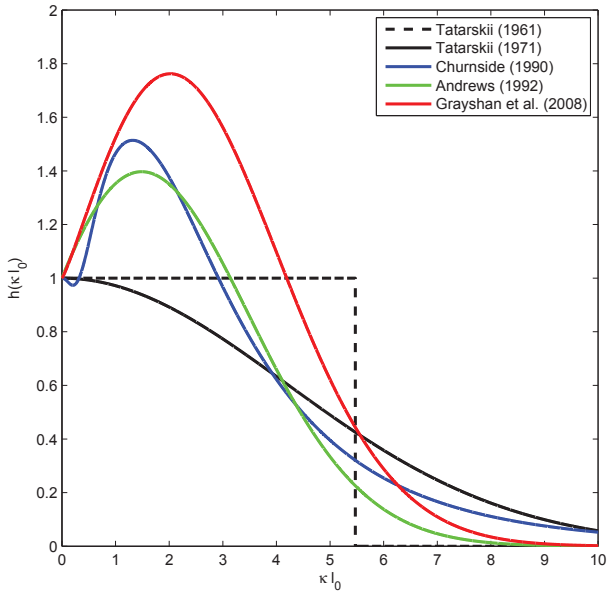

Figure 1: *Five models for the Obukhov-Corrsin-normalized temperature spectrum, where κ is the wave number and l_0 is the inner temperature scale.*

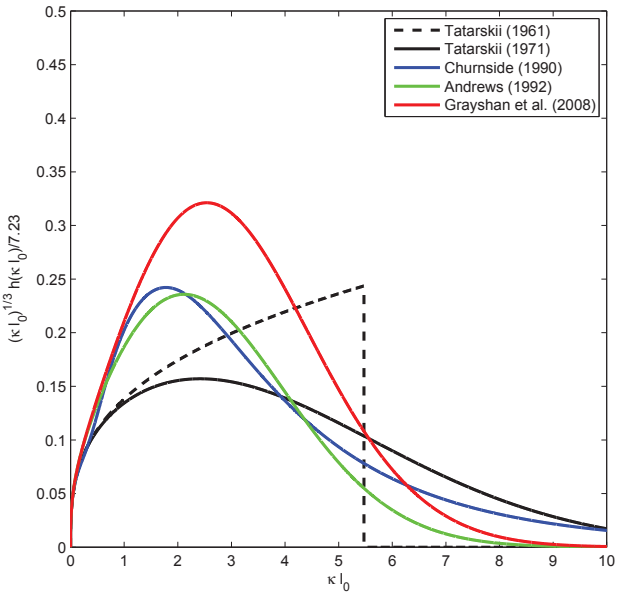

Figure 2: *Normalized dissipation spectra for the five models shown in Figure 1*

References

[1] V. I. Tatarskii, *Wave propagation in a turbulent medium* (McGraw-Hill, New York, 1961).

[2] V. I. Tatarskii, *The effects of the turbulent atmosphere on wave propagation* (Israel Program for Scientific Translation, Jerusalem, Israel, 1971).

[3] A. N. Kolmogorov, "Local structure of turbulence in an incompressible fluid at very high Reynolds numbers," Dokl. Akad. Nauk SSSR **30**, 299–303 (1941).

[4] A. M. Obukhov, "The structure of the temperature field in a turbulent flow," Izv. Akad Nauk SSSR, Ser. Geogr. i Geofiz. **13**, 58–69 (1949).

[5] S. Corrsin, "On the spectrum of isotropic temperature fluctuations in an isotropic turbulence," J. Appl. Phys. **22**, 469–473 (1951).

[6] A. D. Wheelon, *Electromagnetic scintillation — I. Geometrical optics* (Cambridge University Press, Cambridge, United Kingdom, 2001).

[7] A. D. Wheelon, *Electromagnetic scintillation — II. Weak scattering* (Cambridge University Press, Cambridge, United Kingdom, 2003).

[8] L. C. Andrews and R. L. Phillips, *Laser beam propagation through random media* (SPIE Press, Bellingham, Washington, 2005), 2nd ed.

[9] O. Korotkova, *Random light beams: theory and applications* (CRC Press, Boca Raton, 2014).

[10] L. C. Andrews, "Aperture-averaging factor for optical scintillations of plane and spherical waves in the atmosphere," J. Opt. Soc. Am. A **9**, 597–600 (1992).

[11] I. Toselli and O. Korotkova, "General scale-dependent anisotropic turbulence and its impact on free space optical communication system performance," J. Opt. Soc. Am. A **32**, 1017–1025 (2015).

Workshop on
Fundamental Aspects of Geophysical Turbulence II
at NCAR, 5-7 August 2015, Boulder, CO, USA

Large and Small Scale Interaction of Pressure in Turbulent Boundary Layer

Yoshiyui Tsuji[1]
[1] *Graduate School of Engineering, Nagoya University, Nagoya 464-8603, JAPAN*

The interaction between large and small scale motions from the point of pressure fluctuation is studied. Using the small pressure probe, both the static pressure and wall pressure fluctuations were measured inside the zero-pressure gradient boundary layer at relatively high Reynolds numbers. How the large scales in outside affect the small scales near wall is analyzed by means of statistical method. High amplitude positive and negative pressure fluctuations are also analyzed which associate with coherent motions inside the boundary layer. Another interesting aspect is the amplitude modulations of pressure and this topic is reported in this paper.

We have developed a small pressure probe and measured both static and wall pressure simultaneously in turbulent boundary layers up to Reynolds numbers based on the momentum thickness 21000. The statistical features were already reported in the previous studies [1]. Here, in this paper, we investigate the instantaneous feature of turbulence character, especially the large scale and small scale interaction of pressure fluctuations. In Fig.1, we plot the pressure intensity profile, which shows the logarithmic relation;

$$(p^+_{rms})^2 = -A_p \log(y/\delta) + B_p, \tag{1}$$

where A_p and B_p are constant $A_p \simeq 2.52$, $B_p \simeq 2.30$, but B_p depends on flow field. Here, y is a distance from the wall, δ is a boundary layer thickness and subscript + indicates the normalization by inner variables. This relation is similar with that observed in the intensity of stream-wise velocity component predicted by attached eddy model [2];

$$(u^+_{rms})^2 = -A_u \log(y/\delta) + B_u, \tag{2}$$

where A_u is constant but B_u depends on flow field. This velocity logarithmic relation was derived by Perry et al. [3] based on the Townsend !G attached eddy hypothesis, in which the distribution of eddies with a population density inversely proportional to distance from the wall. And in their model, they propose that $(u^+_{rms})^2$ is in proportion to the logarithmic of distance from the wall. From the recent high-Reynolds

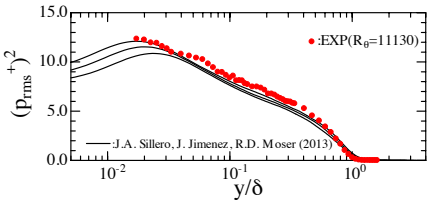

Figure 1: Square of pressure intensity normalized by inner variables at distance from the wall.

number experiments, it was found that large scale motions in overlap region have significant interaction with the motions close to the wall [3]. A series of researches by Melbourne university group have reported the detailed properties of this interaction. This process is conceptually expressed as !Hfootprint !I We generally believe the attached eddy hypothesis relates with this footprint. The large-scale and small-scale interactions, or footprint, are characterized by statistical methods, such as space-time correlation, conditional sampling, joint-probability density functions etc. Among these, one possibility is the amplitude modulation

method [3]. Although there are some discussions about the ability of this method, we apply this to the pressure fluctuation and discuss the similarity and difference with that of velocity fluctuations. A single-point amplitude modulation coefficient, defined as the correlation coefficient between the filtered envelope of the small-scale fluctuations, $E_L(p_s^+)$, and the large-scale component, p_L^+, is calculated by

$$AM(y^+) = \left\langle E_L(p_s^+) p_L^+ \right\rangle / \left[E_{L,rms} p_{L,rms} \right], \tag{3}$$

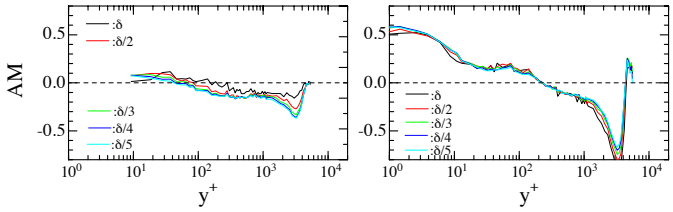

Figure 2: Amplitude modulation coefficient of pressure (left) and velocity (right) at $R_\theta = 11260$

Here, the lower subscript rms means the root mean square of fluctuating quantities. To obtain the term in Eq.3, the pressure fluctuation is decomposed into the large scale p_L and the small scale p_s, by choosing the cut-off wave lengt λ_{th}. The filtered envelope of small-scale contribution was obtained by via a Hilbert transformation. In Fig.2 the amplitude modulation coefficients are plotted against the distance from the wall. The coefficient increases toward the wall, but it is almost constant in the overlap region and extends into the outer region. For the case of velocity signal, AM shows the increasing trend toward the wall, it is almost constant in $30 \leq y^+ \leq 150$ just below the log-region. From these trends, pressure has a different character of velocity fluctuations. That is, the large scale interacts with small scale in a different way in pressure. It is noted that the sign of AM is negative inside the boundary layer, or the large scale interact negatively with small scales. Close to the wall, the coefficient becomes positive but it has a small value. This means the interaction from the outer scale to the wall region is little. These are very interesting and unique features in pressure fluctuations. The similar analysis has already performed in wall pressure signal. It has been discussed that the large scale effect on the wall pressure for a long time. However, the present analysis of AM does not support clearly the large scale contributions. This may be discussed at the conference. The cut-off wavelength is a key parameter for this analysis. The wave number λ_{th} is determined based on the pre-multiplied spectrum contours. It shows the large and small scale energetic modes at position as a function of wave numbers. However, for the simplicity, the cut-off wave numbers are set as $\lambda_{th} = \delta, \delta/2, \delta/5, \delta/10$ in this analysis. In these high Re number experiments, there is little effect of λ_{th} on amplitude modulation coefficients.

As mentioned previously, the pressure intensity shows the logarithmic relation of Eq.1. It is another interesting point for us to investigate how large scales contribute to the pressure intensity profile and attached eddy model can predict the logarithmic relation of pressure. The instantaneous pressure fluctuations are divided into large and small scales by filtering at cut-off wave number λ_{th} and the pressure intensity was reconstructed from smaller and larger wave numbers separately. The detailed things are presented at the conference, but the significant difference from the velocity was found, that is, the logarithmic relation is realized mainly by the small-scale fluctuations in case of pressure.

1 Y. Tsuji, S.Imayama, P.Schlatter, P. H. Alfredsson, A. V. Johansson, I. Marusic, N. Hutchins, and J. Monty, 2012 *Pressure fluctuation in high-Reynolds-number turbulent boundary layer: results from experiments and DNS*, Journal of Turbulence, vol. 13, No. 50, pp.1–19.

2 A. E. Perry, S. Henbest, and M. S. Chong, 1986 *A Theoretical and Experimental Study of Wall Turbulence*, J. Fluid Mech., vol.165, pp.163–199.

3 R.Mathis, N. Hutchins and I. Marusic, 2009 *Large-scale amplitude modulation of the small-scale structures in turbulent boundary layers*, J.Fluid Mech., vol.628, 311.

Workshop on
Fundamental Aspects of Geophysical Turbulence II
at NCAR, 5-7 August 2015, Boulder, CO, USA

Classical Scaling and Intermittency in Strongly Stratified Boussinesq Turbulence

Stephen M. de Bruyn Kops
University of Massachusetts Amherst, Amherst, Massachusetts 01003, U.S.A.

Classical scaling arguments such as those of Kolmogorov, Oboukhov, and Corrsin [1, 2, 3, 4, 5, 6, 7], referred to collectively as KOC, are the basis for many turbulence theories and models. It is valuable for the general understanding of turbulence to know the conditions under which the KOC hypotheses hold. Here, simulated flows are considered that are homogeneous and axisymmetric but strongly affected by a stabilizing density gradient. The term "axisymmetric" refers to the statistics being independent of direction on a horizontal plane rather than to a cylindrical domain.

As noted by Riley and Lindborg [8], if the buoyancy force is important then some of the assumptions of KOC are not met. On the other hand, the -5/3 slope in the horizontal velocity spectra observed in simulations of stratified turbulence more than a decade ago [9] encourages the thought that KOC scaling might be relevant, an idea supported by the geophysical measurements reviewed by Riley and Lindborg [8]. Lindborg [10] hypothesizes that KOC scaling of the spectra holds with roughly the textbook values for the leading multiplicative coefficients. More recent simulations, though, indicate that, while the slope of the velocity spectrum appears to be -5/3 over some range of wave numbers, the slope of the corresponding longitudinal structure function is 2/3 over only part of the corresponding range of separation distances [11]. Statistical analyses suggest that spectra may be more reliable than structure functions for estimating power laws in turbulence [12], and it is well-recognized that one-dimensional spectra alias energy to larger length scales while structure functions aggregate energy below a given length scale [13, 14]. Nevertheless, it is worthwhile to consider implications of KOC scaling beyond those that apply to spectra.

The simulations considered for this study are of forced, homogeneous stratified turbulence resolved on up to $8192 \times 8192 \times 4096$ grid points with buoyancy Reynolds numbers $\mathrm{Re_b} = 13$, 48, and 220. A simulation of isotropic homogeneous turbulence with a mean scalar gradient resolved on 8192^3 grid points is used as a benchmark. The Prandtl number is unity. Based on a wide range of statistics reported in [11], the three stratified simulations can be characterized as strongly, more strongly, and very strongly stratified.

Analysis of the spectra and structure functions (up to third order) of the velocity and scalar fields show that the stratified flows exhibit KOC scaling only for second-order statistics when $\mathrm{Re_b} = 220$; the 4/5 law is not observed. At lower $\mathrm{Re_b}$, the -5/3 slope in the spectra occurs at wave numbers where the bottleneck effect occurs in unstratified cases, and KOC scaling is not observed in any of the structure functions. It is also observed that the bottleneck effect is suppressed by stratification to the extent that there is no "bump" in the compensated velocity or scalar spectra when $\mathrm{Re_b} = 13$.

The refined scaling hypothesis and measures of internal intermittency are also evaluated. For the probability densities functions (p.d.f.s) of the scalar and kinetic energy dissipation rates, the lognormal model works as well for the stratified cases with $\mathrm{Re_b} = 48$ and 220 as it does for the unstratified case. For lower $\mathrm{Re_b}$, the dominance of the vertical derivatives results in p.d.f.s of the dissipation rates tending toward bimodal. The p.d.f.s of the dissipation rates locally averaged over spheres with radius in the inertial range tend toward bimodal regardless of $\mathrm{Re_b}$. There is no broad scaling range, but the intermittency exponents at length scales near the Taylor length are in the range of 0.25 ± 0.05 and 0.35 ± 0.1 for the velocity and scalar, respectively.

References

[1] A. N. Kolmogorov. Local structure of turbulence in an incompressible fluid at very high Reynolds numbers. *Dokl. Akad. Nauk SSSR*, 30:299–303, 1941.

[2] A. M. Oboukhov. Spectral energy distribution in a turbulent flow. *Dokl. Akad. Nauk. SSSR*, 32:22–24, 1941a.

[3] A. M. Oboukhov. Spectral energy distribution in a turbulent flow. *Izv. Akad. Nauk. SSSR, Ser. Geogr. i. Geofiz*, 5:453–466, 1941b.

[4] A. M. Oboukhov. Structure of temperature field in a turbulent flow. *Izv. Akad. Nauk. SSSR, Geogr. i Geofiz*, 13:58, 1949.

[5] S. Corrsin. On the spectrum of isotropic temperature fluctuations in an isotropic turbulence. *J. Appl. Phys.*, 22:469–472, 1951.

[6] A. N. Kolmogorov. A refinement of previous hypotheses concerning the local structure of turbulence in a viscous incompressible fluid at high Reynolds number. *J. Fluid Mech.*, 13:82–85, 1962.

[7] A. M. Oboukhov. Some specific features of atmospheric turbulence. *J. Fluid Mech.*, 13:77–81, 1962.

[8] J. J. Riley and E. Lindborg. Stratified turbulence: A possible interpretation of some geophysical turbulence measurements. *J. Atmos. Sci.*, 65(7):2416–2424, 2008.

[9] J. J. Riley and S. M. de Bruyn Kops. Dynamics of turbulence strongly influenced by buoyancy. *Phys. of Fluids*, 15(7):2047–2059, 2003.

[10] E. Lindborg. The energy cascade in a strongly stratified fluid. *J. Fluid Mech.*, 550:207–242, 2006.

[11] S. Almalkie and S. M. de Bruyn Kops. Kinetic energy dynamics in forced, homogeneous, and axisymmetric stably stratified turbulence. *J. Turbulence*, 13(29):1–29, 2012.

[12] G. A. Nichols-Pagel, D. B. Percival, P. G. Reinhall, and J. J. Riley. Should structure functions be used to estimate power laws in turbulence? A comparative study. *Physica D*, 237:665–677, 2008.

[13] A. A. Townsend. *The structure of turbulent shear flows*. Cambridge University Press, 1956.

[14] P. A. Davidson and B. R. Pearson. The structure of turbulent shear flows. *Phys. Rev. Lett.*, 95:214501, 2005.

Workshop on
Fundamental Aspects of Geophysical Turbulence II
at NCAR, 5-7 August 2015, Boulder, CO, USA

Physical- and eddy-viscosity effects in simulations of stratified turbulence

Michael Waite[1] **and Sina Khani**[1,2]
[1] *University of Waterloo, Waterloo, Ontario, N2L 3G1, CANADA*
[2] *École Polytechnique Fédérale de Lausanne, CH-1015, SWITZERLAND*

Stratified turbulence is turbulence in a stably stratified fluid with weak or no rotation. Since the Coriolis parameter is much less than the buoyancy frequency N over much of the atmosphere and ocean, stratified turbulence has been used as a model for atmospheric and oceanic turbulence at intermediate and small length scales. In the atmosphere, it has been hypothesized that stratified turbulence might explain the energy cascade through the mesoscale, from scales of $O(100)$ down to $O(1)$ km [1, 2].

Stratified turbulence occurs in the parameter regime of small Froude number $Fr = U/NL$ ("stratified") and large Reynolds number $Re = UL/\nu$ ("turbulence"), where U is the characteristic horizontal velocity, L is the characteristic horizontal length, and ν is the kinematic viscosity. Stratification inhibits vertical motion, leading to a layerwise structure of pancake vortices with thickness on the order of the buoyancy scale $L_b = 2\pi U/N$. As a result, the thickness of the layers decreases with increasing stratification. Ultimately, if Fr is decreased at fixed Re, the vortices become so thin that they are damped by viscosity. Therefore, it is not sufficient to have small Fr and large Re, because smaller Fr require larger Re. Instead, the buoyancy Reynolds number $Re_b = Fr^2 Re$ must also be large. The importance of Re_b in stratified turbulence has been verified in several studies (e.g. [3]). The requirement of very large $Re \gg Fr^{-2}$ presents a significant challenge for performing direct numerical simulations (DNS) of stratified turbulence, in which all scales down to the viscous dissipation scale are resolved.

Large eddy simulation (LES) is an alternative approach to DNS that employs coarser numerical grids. Instead of resolving all scales down to the viscous scale, the effects of unresolved sub-grid-scale eddies are parameterized, often with an eddy viscosity model. In principle, this approach allows high-Re simulations to be performed with lower resolution than DNS. However, in practice, LES for stratified turbulence suffers from similar challenges as DNS. As Fr decreases with fixed grid resolution, the thickness of the pancake vortices decreases until it approaches the grid spacing. Since the eddy viscosity damps grid-scale motions, it is likely that problems will emerge in this limit, analogous to the damping of thin vortices by viscosity in DNS with small Re_b. This hypothesis is investigated in this work.

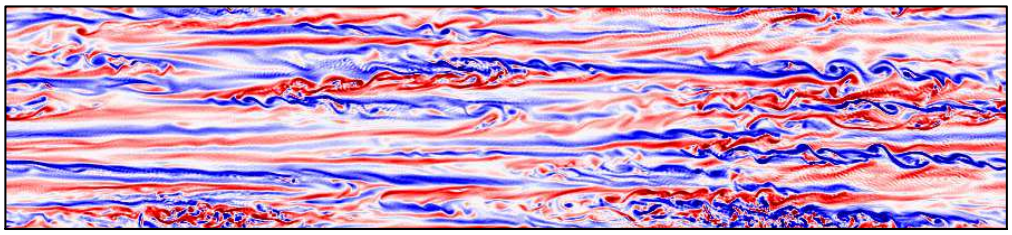

Figure 1: *Snapshot of a vertical (x,z) slice of the y-component of vorticity ω_y in a DNS with $Fr = 0.02$ and $Re_b \approx 2$. In some regions, the pancake vortices are smooth and viscously coupled; other regions have KH instabilities and patches of small-scale turbulence.*

This talk will have two parts. First, I will present DNS of stratified turbulence with $Re_b \sim O(1)$. While this regime is not directly relevant to atmospheric and oceanic turbulence, which have $Re_b \gg 1$, it is

important to understand how viscous effects are manifested because similar results occur in under-resolved LES (see below). When $Re_b > 1$, simulations show energy spectra with an approximately $-5/3$ slope in horizontal wavenumber [3]. Kelvin–Helmholtz (KH) instabilities form on the pancake vortices (figure 1), leading to regions of small-scale turbulence and a spectral bump at the buoyancy scale. Higher-order terms in the potential vorticity (PV) are important in this regime. As Re_b decreases through $O(1)$, the energy spectrum steepens, KH instabilities are suppressed, and the linear part of the PV becomes dominant. While these effects sound superficially like a transition to two-dimensional turbulence [1], the small-Re_b regime is actually quite different, because viscous damping of small vertical scales shuts down the turbulent cascade over a wide range of horizontal scales. These DNS results are from [4, 5].

In the second part of this talk, I will present LES of stratified turbulence, which will be interpreted in light of the DNS discussed above. Three LES schemes will be considered and compared: the Kraichnan [6], Smagorinsky [7], and dynamic Smagorinsky [8] models. The ability of these schemes to capture basic characteristics of stratified turbulence – including an approximately -5/3 energy spectrum in horizontal wavenumber, a spectral bump around L_b, and resolved KH instabilities and overturning – is investigated and compared. We find that these schemes work well when the buoyancy scale L_b is resolved, but some schemes require more resolution of L_b than others. In particular, we obtain reasonable results when the grid spacing Δ satisfies $\Delta/L_b < 0.47$ for the Kraichnan model, 0.17 for the Smagorinsky model, and 0.24 for the dynamic Smagorinsky model. In particular, despite requiring almost twice as much work per timestep at the same resolution, the dynamic Smagorinsky model provides an improvement over the regular Smagorinsky model because it can be applied with lower grid resolution. The LES results are from [9, 10].

References

[1] D. K. Lilly 1983 *Stratified turbulence and the mesoscale variability of the atmosphere*, *J. Atmos. Sci.* **40**, 749-761.

[2] J. J. Riley and E. Lindborg 2008 *Stratified turbulence: a possible interpretation of some geophysical turbulence measurements*, *J. Atmos. Sci.* **65**, 2416–2424.

[3] G. Brethouwer, P. Billant, E. Lindborg and J. M. Chomaz 2007 *Scaling analysis and simulation of strongly stratified turbulent flows*, *J. Fluid Mech.* **585**, 343–368.

[4] M. L. Waite 2013 *Potential enstrophy in stratified turbulence*, *J. Fluid Mech.* **722**, R4.

[5] M. L. Waite 2014 *Direct numerical simulations of laboratory-scale stratified turbulence*, *Modelling Atmospheric and Oceanic Flows: Insights from Laboratory Experiments and Numerical Simulations* (American Geophysical Union) 159–175.

[6] R. H. Kraichnan 1976 *Eddy viscosity in two and three dimensions*, *J. Atmos. Sci.* **33**, 1521–1536.

[7] J. Smagorinsky 1963 *General circulation experiments with the primitive equations. I. The basic experiment*, *Mon. Weather Rev.* **91**, 99-1-64.

[8] M. Germano, U. Piomelli, P. Moin and W. H. Cabot 1991 *A dynamic subgrid-scale eddy viscosity model*, *Phys. Fluids A* **3**, 1760–1765.

[9] S. Khani and M. L. Waite 2014 *Buoyancy scale effects in large-eddy simulations of stratified turbulence*, *J. Fluid Mech.* **754**, 75–97.

[10] S. Khani and M. L. Waite 2015 *Large eddy simulation of stratified turbulence: the dynamic Smagorinsky model*, *J. Fluid Mech.* **773**, 327-344.

Workshop on
Fundamental Aspects of Geophysical Turbulence II
at NCAR, 5-7 August 2015, Boulder, CO, USA

Insights into the performance of the QNSE-EDMF scheme in stable and unstable conditions

Esa-Matti Tastula[1], Boris Galperin[1], Margaret A. Lemone[2], Jimy, Dudhia[2], Semion Sukoriansky[3] and Timo Vihma[4]
[1] *College of Marine Science, University of South Florida, St. Petersburg, Florida, U.S.A.*
[2] *National Center for Atmospheric, Boulder, CO, U.S.A.*
[3] *Ben-Gurion University of the Negev, Department Mechanical Engineering, Beer-Sheva, Israel*
[4] *Finnish Meteorological Institute, Helsinki, Finland*

WRF 3D simulations for CASES97 and CASES99 field campaigns addressed the performance of the QNSE-EDMF PBL scheme [1, 2] in both stable and unstable conditions. For the stable part, the objective was to investigate the reasons for the previously discovered excessive mixing in the local QNSE part of the scheme in near-neutral conditions [3]. The results demonstrate that this phenomenon can be attributed to the applied turbulent kinetic energy subroutine and the choice of the neutral turbulent Prandtl number in the scheme. For the unstable part, the importance of the mass-flux component in the QNSE-EDMF scheme was evaluated. The inclusion of the mass flux component improved virtual temperature, and in particular, mixing ratio profile error statistics. Similar improvements were not as clearly visible in turbulent flux profiles. The influence of the mass flux scheme extends to mesoscale circulation features, which were greatly altered by both the inclusion of mass flux and a change made to the entrainment/detrainment formulation. Adding mass flux based clouds to the radiation calculations improved the time and space averaged incoming shortwave flux in the model.

References

[1] Tastula, E.-M., Galperin, B., Dudhia, J., LeMone, M.A., Sukoriansky, S., and Vihma, T., 2015: Methodical assessment of the differences between the QNSE and MYJ PBL schemes for stable conditions. Q.J.R. Meteorol. Soc.. doi: 10.1002/qj.2503

[2] Pergaud, J., Masson V., Malardel S., and Couvreux F., 2009: A parameterization of dry thermals and shallow cumuli for mesoscale numerical weather prediction. Boundary-Layer Meteorology, 132, 83-106.

[3] LeMone M.A., Tewari M., Chen F., and Dudhia J., 2014, Objectively Determined Fair-Weather NBL Features in ARW-WRF and Their Comparison to CASES-97 Observations.Mon.Wea.Rev., 142, 27092732. doi: http://dx.doi.org/10.1175/MWR-D-13-00358.1